Master of Science Thesis in Electrical Engineering
Department of Electrical Engineering, Linköping University, 2019

Exhaust Temperature Modeling and Optimal Control of Catalytic Converter Heating

Victor Petersson

Master of Science Thesis in Electrical Engineering

Exhaust Temperature Modeling and Optimal Control of Catalytic Converter Heating:

Victor Petersson

LiTH-ISY-EX--19/5237--SE

Supervisor: **Olov Holmer**
ISY, Linköping Universitet

Examiner: **Lars Eriksson**
ISY, Linköping Universitet

Division of Automatic Control
Department of Electrical Engineering
Linköping University
SE-581 83 Linköping, Sweden

Abstract

After reaching its light-off temperature, the catalytic aftertreatment system plays a major part in maintaining emissions at low levels for vehicles equipped with combustion engines. In this thesis, modelling of the exhaust gas temperature is investigated along with optimal control strategy for variable ignition and exhaust valve opening angles for optimal catalytic converter heating.

Models for exhaust gas temperature and mass flow are presented and validated against measurement data. According to the model validation, the proposed models capture variations in ignition and exhaust valve opening angles well. Optimal control strategy for the ignition and exhaust valve opening angles to heat the catalytic converter to a predetermined temperature in the most fuel and time optimal ways are investigated by implementation of the validated models.

Optimal control analysis indicates that with open wastegate, the heating time for the catalytic converter can be reduced by up to 16.4% and the accumulated fuel to reach the desired temperature can be reduced by up to 4.6%, compared to the case with ignition and exhaust valve opening angles fixed at nominal values. With closed wastegate the corresponding figures are 16.4% and 4.7%. By also including control of the variable λ-value, the heating time can be further reduced by up to 19.8%, and the accumulated fuel consumption by up to 9.5% with open wastegate. With closed wastegate the corresponding figures are 20.1% decrease in heating time, and 9.8% decrease in accumulated fuel consumption.

Acknowledgments

I would like to thank my examiner Lars Eriksson and supervisor Olov Holmer who made this thesis possible, and for giving me guidance throughout the project. I would also like to thank Tobias Lindell for his help in the engine laboratory. Finally I would like to thank my family and friends who have shown a lot of support and encouragement throughout my education.

Linköping, June 2019
Victor Petersson

Contents

Notation

Abbreviations

Abbreviation	Description
SI	Spark ignition
VVT	Variable valve timing
VCT	Variable cam timing
GDI	Gasoline direct injection
TDC	Top dead center
BTDC	Before top dead center
ATDC	After top dead center
MVEM	Mean value engine models
OCP	Optimal control problem
NLP	Nonlinear programming
IG	Ignition
EVO	Exhaust valve opening
CAD	Crank angle degrees
MAE	Mean average error

1 Introduction

1.1 Purpose and goal

For vehicles equipped with combustion engines the catalytic aftertreatment system plays a major part in maintaining the emissions at low levels. For a catalytic converter to be functioning and reducing the emissions as intended it is necessary that the temperature of the catalytic converter has reached a certain level at which the chemical reactions reducing the emissions start to occur at a significant level. This means that during the initial driving phase after a cold start, prior to the catalytic converter reaching the so called *light-off temperature*, the emissions from the vehicle are higher compared to the driving phase after the catalytic converter has reached the *light-off temperature*. Therefore, the time required for the catalytic converter to reach the *light-off temperature* can in some cases have a big influence on the accumulated emissions from the vehicle. In the light of this, it is of interest to research methods that allows faster heating of the catalytic converter during cold start. The purpose of this master thesis is to research whether if, and how, variable ignition timing and variable valve timing, *VVT*, on the exhaust side of the cylinder can be used in an SI-engine to control the heating time of the catalytic converter.

The goal of this master thesis can be divided into three items, presented below. The goals are related partly to modelling of the relevant subsystems, and partly to optimal control strategy based on the developed models.

- Obtain models that include variable ignition and valve timings and describe the exhaust gas temperatures prior and after the turbine in a turbocharged SI-engine.
- Based on the developed models, minimize the heating time of the catalytic converter and accumulated fuel consumption through either development

of a controller or obtaining a trajectory of control signals from optimal control analysis, where variable ignition and valve timings are utilized.

- Analyze how variable ignition and valve timings can be used to control the heating of the catalytic converter. Make comparisons to previously obtained research results where a two-phase behavior has been observed for optimal catalytic converter heating.

1.2 Problem formulation

In the light of the purpose and goal previously presented, a problem formulation for this master thesis has been formulated, presented below.

- How can the cylinder-out and turbine outlet exhaust gas temperatures be modelled to include ignition angle and variable valve timing?
- How can the obtained models be used to generate control signals for ignition angle and valve timings such that the fuel consumption and heating time for the catalytic converter can be minimized?
- How is the catalytic converter heated in the shortest time using variable ignition and valve timings? How is the catalytic converter heated in the most fuel efficient way using variable ignition and valve timings? How does the observed behaviour relate to behaviour observed in previous research regarding this topic?

1.3 Delimitations

Due to time constraints some delimitations are adopted within this project. To obtain a catalytic converter model which is both simple to implement for optimal control and does not contain a lot of parameters to estimate, the premise is made that the different chemical reactions within the catalytic converter are not to be modelled seperately. Instead it is expected that a model for the catalytic converter is used where the various chemical reactions are lumped together as one single parameter. This delimitation is motivated by the time constraint on the project and the various possible difficulties a too complex model can introduce to the project.

A second delimitation adopted within this project is to only consider the case of conventional turbocharging. This means that for this project all modelling and analyses are performed for the case where a turbine and compressor are mechanically coupled, and the exhaust gases will cause the turbine to rotate and drive the compressor which compresses the air on the intake side of the cylinder. Other types of supercharging, for example mechanical supercharging, two stage turbocharging, engine driven compressor and turbocharger etc., are not considered within this project. This delimitation is motivated both by the projects time

constraint and that the experimental setup used to perform measurements in this project only allows measurements on a conventional turbocharged engine.

A third delimitation is that the only variable valve timing included is the exhaust valve opening timing, since this is believed to be the valve timing with the most influence on exhaust gas temperature.

1.4 Outline

A short overview of the outline of this thesis is presented below.

Chapter 1. Introduction Presentation of the purpose, goals, problem formulation and delimitations of this thesis.

Chapter 2. Related research A summary of previous research related to the topic of this thesis.

Chapter 3. Modelling An overview of modelled subsystems and descriptions of the proposed models.

Chapter 4. Optimal control A presentation of the optimal control problems that has been analyzed.

Chapter 5. Measurements The test setup is described and the performed measurements are presented.

Chapter 6. Model validation The proposed models are validated against measurement data.

Chapter 7. Results The obtained results from the optimal control analysis are presented.

Chapter 8. Discussion, conclusions and future work The obtained results are discussed and based on the presented work conclusions are drawn and suggestions on future work are presented.

2

Related research

In this chapter research related to this thesis project is presented. The chapter is divided into two sections. In the first section research related to modelling of exhaust gas temperatures is briefly summarized, and in the second section research with focus on heating of the catalytic converter is presented.

2.1 Modelling

2.1.1 Modelling of cylinder and cylinder-out temperature

To be able to model the exhaust gas temperatures after the cylinder, models describing the in-cylinder process are necessary. In [8] an analytical model for cylinder pressure, obtained from parameterizing the ideal Otto cycle, is presented and validated. The model takes the angle of ignition into account and describes the cylinder pressure in terms of the position of the piston as well as the temperature and pressure in the cylinder inlet side. The model utilizes the Vibe function to interpolate between the asymptotic pressures. The model is validated for operating conditions close to stoichiometric conditions.

A model for the effect of ignition angle on efficiency and torque is presented and validated in [2]. The proposed model is a two-zoned model also using the Vibe function to model the combustion process. The model consists of a system of differential equations requiring a fifth order Runge-Kutta method to obtain numerical solutions.

A model for the mass of air and residual gases in the cylinder is presented in [19]. The model takes VVT on both the intake and exhaust side into account and utilizes the engine speed, intake manifold pressure and valve positions. Further

models for air and residual gas masses in the cylinder are presented in [21] and [9]. Unlike [19] the model in [21] utilizes in-cylinder pressure, intake manifold pressure and intake manifold temperature to estimate the air mass. The models in [21] and [9] are extended in [31] to also include VCT.

In [10] a model is presented for exhaust gas temperature expressed in term of in-cylinder pressure, engine speed and exhaust lambda. The model assumes an isentropic expansion over the exhaust valve. By using a nodal thermal model the gas temperature drop along the exhaust runner and manifold is estimated.

In [13] a static non-linear model for the engine is presented, based on sub-models presented in [23]. The cylinder model consists of several sub-models. A throttle model is used to model the intake manifold pressure and the air mass flow is obtained through the use of the ideal gas law. Three sub-models for torque, pumping and friction is used to model the engine gross work. Losses due to combustion efficiency, ignition efficiency, maximum thermodynamic efficiency and fuel evaporation are considered to obtain an expression for the cylinder-out temperature.

2.1.2 Modelling of temperature between cylinder and turbine

Having a model describing the temperature change between the cylinder and the turbine is of interest to be able to model the final exhaust temperature reaching the catalytic converter. In [7] three models for the temperature drop along the exhaust pipe are suggested. All three models are intended to be used as mean value models, and the model validation shows that the models exhibit results that agrees well with the measured temperatures. A temperature model for the exhaust system is also presented in [30], and in [14] a model for dual wall exhaust system is presented.

2.1.3 Modelling of temperature after turbine

In [25] a non-adiabatic model for the turbine heat transfer is presented. In [22], turbine and compressor models are presented together with an overview of curve fitting methods for compressors and turbines. The turbocharger heat transfer is also investigated in [1]. In this paper it is concluded that the heat transfer is dependant on the turbine inlet temperature, the ambient temperature and the velocity of the air around the turbine. It is also concluded that the turbine outlet temperature is closely related to the pressure ratio over the turbine, the turbine inlet temperature, the turbine wall temperature and the surrounding ambient temperature. Turbocharger heat transfer is investigated and modelled in [27] with good accuracy. In [23] a lot of research related to modelling of turbines and compressors are compiled.

2.1.4 Modelling of catalytic converter temperature

In [26] a semi-empirical temperature model for a three-way catalytic converter is presented. The model is derived from partial differential equations describing the energy balance in the catalytic converter. The model is simplified through the lumping of all terms describing the various chemical reactions in the catalytic converter. A more extensive model for the catalytic converter is presented in [5] where corresponding simplification of the chemical reactions is not performed. Another model, also quite extensive, is presented in [24]. This model is based on the mass and energy balances for 15 different chemical reactions in the catalytic converter. A fourth model for the catalytic converter is presented in [13]. This model describes the physics of the catalytic converter using partial differential equation and does not require the chemical reactions in the catalytic converter to be handled individually.

2.2 Control of catalytic converter temperature

2.2.1 Experimental studies

In [28] experimental studies are performed with the purpose of investigating how variable ignition angle affects the properties of a SI engine. In the study it is concluded that moving the ignition angle closer to TDC (Top Dead Center) causes the exhaust gas temperatures to increase. In [20] and [15] similar studies are performed where it is concluded that moving the ignition angle closer to TDC will decrease the thermal efficiency of the engine.

In [11] the optimal control of ignition retardation is investigated to minimize hydrocarbon emissions and engine fuel consumption. In the study, fixed ignition angle is used during cold start of a GDI engine, and it is concluded that using maximum ignition retardation is optimal to minimize the accumulated hydrocarbon emissions and fuel consumption to reach a predetermined temperature of the catalytic converter.

In [17] a study is presented where electrical heating of the catalytic converter is compared to heating by later ignition angle. In the paper it is shown that when moving the ignition angle 10 degrees closer to TDC the light-off time becomes approximately 50 % shorter.

2.2.2 Optimal control

In [4] a method using iterative dynamic programming is presented as a method to obtain an optimal control strategy for minimized accumulated fuel consumption at engine cold start for a gasoline powered vehicle. Based on the result the conclusion is drawn that using lambda, ignition angle and VVT the accumulated fuel consumption can be decreased. Iterative dynamic programming is also used

in [18] to study optimal control strategies for SI engines at cold start.

In [13] optimal heating of the catalytic converter is obtained by formulating a time discrete optimization problem which is solved using CasADi [3] and IPOPT [29].

2.2.3 Control strategies

According to [23] open loop control using intake manifold pressure and engine speed is the most common strategy for ignition angle control. The aim of this control is to position the ignition angle as close as possible to the optimal value with the purpose of maximizing the engine efficiency.

In [4] an alternative method is presented where optimal trajectories for ignition angle, lambda and VVT, obtained from iterative dynamic programming, are used as open loop control signals in an engine test stand. In [16], LQR and MPC are both proposed as suitable controllers to use for optimal engine control purposes. Both these controls are evaluated and LQR is believed to be the better choice.

3

Modelling

This section presents the suggested models for the different subsystems. The suggested models falls within the category *mean value engine models*, which from now on will be abbreviated as *MVEM*, meaning that the models describes variations in the system at a frequency slower than the engine cycle [23]. In this chapter a brief overview of the modelled system is first presented, followed by presentations of the proposed models for the different components.

3.1 System overview

A schematic illustration of the system and its components are presented in Figure 3.1. The system consists of the air filter, compressor, intercooler, throttle, intake manifold, cylinder, exhaust manifold, turbine, wastegate, pipe section and catalytic converter.

Within this project, not all components included in the system are to be modelled. The air filter and intercooler are not modelled, since these are believed to have minor influence on the exhaust gas temperature in the system. It is further assumed that the throttle is perfectly controlled to always provide the desired air mass flow to maintain constant λ for a given desired engine torque. With this assumption, a throttle model is not required to model neither the air nor fuel mass flow in the system.

Within this project, the components which require modelling are therefore the intake manifold, cylinder, exhaust manifold, turbine, compressor, wastegate, pipe section and catalytic converter.

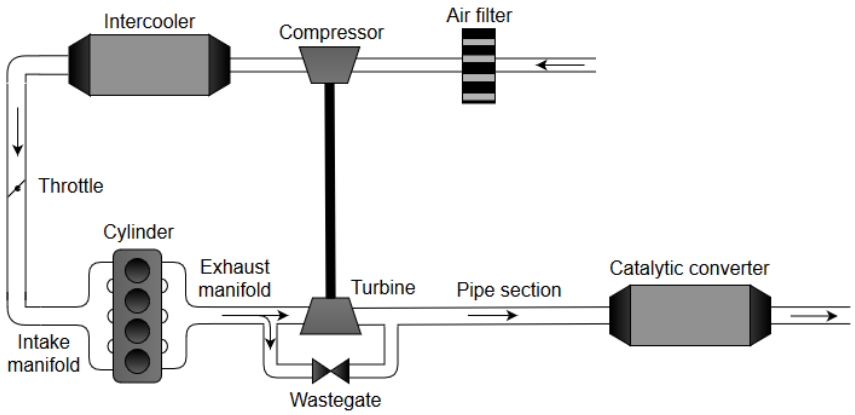

Figure 3.1: *A schematic illustration of the different components that make up the system to be modelled.*

3.2 Otto cycle

3.2.1 Inclusion of ignition and exhaust valve opening angles

The modelling of the engine operating cycle is based on the idea of the ideal Otto cycle. To account for the effects due to variations in ignition and exhaust valve opening angles, some modifications to the cycle are introduced. Instead of assuming the compression ratio, commonly denoted r_c, as a constant, the approach in this project is to treat it as having different values during the compression and expansion strokes.

In the common ideal Otto cycle, the compression ratio is defined according to (3.1) as the ratio between the compressed volume, V_c, and the fully expanded volume, $V_d + V_c$, where V_d is the volume displaced by the cylinder [23].

$$r_c = \frac{V_c + V_d}{V_c} \tag{3.1}$$

In (3.1) both V_c and V_d are assumed to be constant. The approach in this project is to instead treat the compressed and expanded volumes as functions of the deviations in ignition and exhaust valve opening angles, $\Delta\theta_{ig}$ and $\Delta\theta_{evo}$. The angle deviations are defined according to (3.2), where ${\theta_{ig}}^*$ and ${\theta_{evo}}^*$ are the nominal values for ignition angle and exhaust valve opening angle respectively.

$$\begin{cases} \Delta\theta_{ig} = \theta_{ig} - {\theta_{ig}}^* \\ \Delta\theta_{evo} = {\theta_{evo}}^* - \theta_{evo} \end{cases} \tag{3.2}$$

By the definitions in (3.2) positive values for $\Delta\theta_{ig}$ and $\Delta\theta_{evo}$ corresponds to ignition angle och exhaust valve opening located closer to TDC than the nominal

values.

In order to express the compressed and expanded volumes as functions of deviations from nominal angle values, the common expression for the cylinder volume as a function of crank angle presented in (3.3) is used [23].

$$V(\theta) = V_d \cdot \left(\frac{1}{r_c - 1} + \frac{1}{2} \cdot \left(\frac{l}{a} + 1 - cos(\theta) - \sqrt{\left(\frac{l}{a} \right)^2 - sin^2(\theta)} \right) \right) \tag{3.3}$$

In order to use the volume expression in (3.3) polynomial expressions of the angle deviations in (3.2) are used instead of the actual crank angle θ.

$$\begin{cases} \theta_{MB50} = c_{ig,1} + c_{ig,2} \cdot \Delta\theta_{ig} \\ \theta_{evo} = c_{evo,1} + c_{evo,2} \cdot \Delta\theta_{evo} \end{cases} \tag{3.4}$$

Here, l and a are the length of the connecting rod and crank radius respectively. In (3.4) the notation θ_{MB50} is used to represent the angle for the compressed volume V_{MB50}, where MB50 is short for **M**ass **B**urned **50** %, since this is approximately the volume where 50 % of the fuel in cylinder has been burned. The volume at the end of the expansion stroke is denoted V_{evo}. By inserting the polynomial expression in (3.4) into the expression for cylinder volume in (3.3) the compressed and expanded volumes V_{MB50} and V_{evo} as functions of angle deviations are obtained according to (3.5) and (3.6).

$$\begin{aligned} V_{MB50}(\Delta\theta_{ig}) = & V_d \cdot \left(\frac{1}{r_c - 1} + \frac{1}{2} \cdot \left(\frac{l}{a} + 1 - cos(c_{ig,1} + c_{ig,2} \cdot \Delta\theta_{ig}) \right. \right. \\ & \left. \left. - \sqrt{\left(\frac{l}{a} \right)^2 - sin^2(c_{ig,1} + c_{ig,2} \cdot \Delta\theta_{ig})} \right) \right) \end{aligned} \tag{3.5}$$

$$\begin{aligned} V_{evo}(\Delta\theta_{evo}) = & V_d \cdot \left(\frac{1}{r_c - 1} + \frac{1}{2} \cdot \left(\frac{l}{a} + 1 - cos(c_{evo,1} + c_{evo,2} \cdot \Delta\theta_{evo}) \right. \right. \\ & \left. \left. - \sqrt{\left(\frac{l}{a} \right)^2 - sin^2(c_{evo,1} + c_{evo,2} \cdot \Delta\theta_{evo})} \right) \right) \end{aligned} \tag{3.6}$$

As mentioned previously, the approach used within this project modifies the ideal Otto cycle and assumes different volume ratios for the compression and expansion strokes. The notations used are r_{comp} and r_{exp} for the compression and expansion stroke respectively. It is assumed that the compression starts at the full expansion volume $V_d + V_c$ and ends at the volume V_{MB50}. The expansion stroke is assumed to start at the volume V_{MB50} and ends at V_{evo}. The compression and expansion ratios are therefore defined according to (3.7)

$$\begin{cases} r_{comp} = \dfrac{V_d + V_c}{V_{MB50}(\Delta\theta_{ig})} \\ r_{exp} = \dfrac{V_{evo}(\Delta\theta_{evo})}{V_{MB50}(\Delta\theta_{ig})} \end{cases} \tag{3.7}$$

The difference between the ideal Otto cycle and the modified cycle is illustrated in Figure 3.2 where the pumping work, presented in Section 3.2.3, is also included.

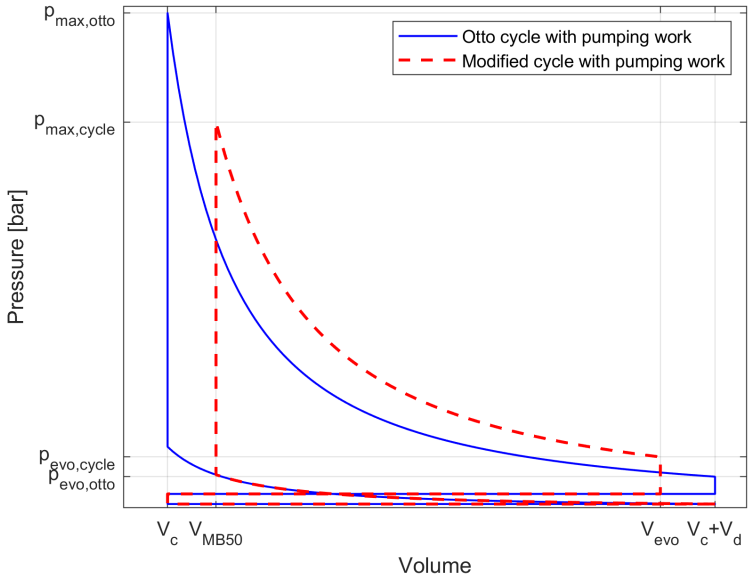

Figure 3.2: *A graphical presentation of the ideal Otto cycle and the presented modified cycle with pumping work included.*

3.2.2 Effect on cycle efficiency

Modifying the ideal Otto cycle according to the method presented in Section 3.2, a new expression for the cycle efficiency is obtained. The efficiency of the ideal Otto cycle is denoted η_{otto} and of the modified cycle is simply denoted η_{cycle}. The expressions for the efficiencies are presented in (3.8).

$$\eta_{otto} = 1 - \frac{1}{{r_c}^{\gamma-1}} \tag{3.8a}$$

$$\eta_{cycle} = 1 - \left(\frac{V_{MB50}}{V_{evo}}\right)^{\gamma-1} - \frac{(1-(A/F)_s \cdot \lambda)\cdot c_v}{q_{LHV}} \cdot \left(\left(\frac{V_c + V_d}{V_{evo}}\right)^{\gamma-1} - 1\right) \cdot T_{im} \tag{3.8b}$$

For a more thorough presentation of the ideal Otto cycle and the derivation of its efficiency in (3.8a), the reader is refereed to other literature, for example [23]. The full derivation of the modified cycle efficiency η_{cycle} is presented in Appendix A.

3.2.3 Effect on pumping work

A common model for the engine pumping work is presented in (3.9) [23].

$$W_{ip} = V_d \cdot (p_{em} - p_{im}) \tag{3.9}$$

In Figure 3.3 the pumping work from Figure 3.2 is illustrated in close up, where it can be observed that the pumping losses are affected by the exhaust valve opening volume, V_{evo}, for the modified cycle.

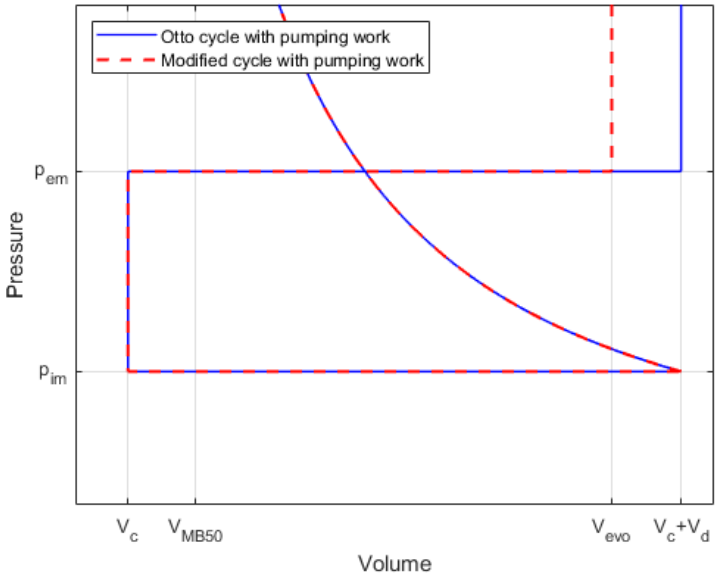

Figure 3.3: *A graphical presentation of the pumping work with and without the presented modifications.*

In (3.10) a pumping work model similar to (3.9) is presented for the modified cycle.

$$W_{ip} = W_{ip}(\theta_{evo}) = (V_{evo}(\theta_{evo}) - V_c) \cdot p_{em} - V_d \cdot p_{im} \tag{3.10}$$

3.3 Cylinder model

3.3.1 Cylinder-out temperature

The modelling of the cylinder-out temperature is based on the enthalpy and temperature equilibrium in (3.11) [23].

$$c_p(\dot{m}_{air} + \dot{m}_f) \cdot T_{eo} = \dot{m}_{air} c_p T_{im} + \dot{m}_f c_p T_f + \dot{m}_f q_{LHV} \eta_\lambda - x_e \dot{m}_f h_{fg} - \dot{W}_{ig} - \dot{Q}_{ht} \tag{3.11}$$

The left hand side of (3.11) is the enthalpy flow out of the cylinder. The first term on the right hand side represent the enthalpy flow of the air entering the intake valve, and the second term is the enthalpy flow of the fuel entering the cylinder through the fuel injector. The third term on the right hand side represents the chemical energy released through the combustion of the fuel. The fourth term on the right hand side represent the heat loss due to energy consumed by the evaporation of the injected fuel. The fifth term on the right hand side is the energy loss due to work produced on the piston, and the last term is energy loss due to heat exchange with the environment. By a simple rearrangement of (3.11) the expression for cylinder out temperature T_{eo} in (3.12) is obtained.

$$T_{eo} = \frac{\dot{m}_{air} c_p T_{im} + \dot{m}_f c_p T_f + \dot{m}_f q_{LHV} \eta_\lambda - x_e \dot{m}_f h_{fg} - \dot{W}_{ig} - \dot{Q}_{ht}}{c_p(\dot{m}_{air} + \dot{m}_f)} \tag{3.12}$$

In (3.12) one can observe that the engine-out temperature is directly affected by the air and fuel mass flows, $\dot{m}_{air}$ and $\dot{m}_f$, the work production on the piston, $\dot{W}_{ig}$, and the heat exchange with the surrounding, $\dot{Q}_{ht}$. It is therefore of interest to find sub-models describing how these quantities are affected by ignition and exhaust valve opening angles.

3.3.2 Gross work model

The model for the indicated gross work is based on the premise that three different types of work is produced by the engine, as proposed in [23]. Firstly, work is required to produce the actual torque delivered by the engine. Secondly, work is required to overcome the friction between the piston and the internal cylinder wall, and lastly work is required to pump the exhaust gases out from the cylinder during the exhaust stroke. The total power required from the engine, W_{ig}, is modelled according to

$$\dot{W}_{ig} = \dot{W}_{ig}(\theta_{evo}) = \frac{N_e}{n_r} \cdot \left(2\pi n_r M_e + W_{ip}(\theta_{evo}) + W_{fr} \right) \tag{3.13}$$

where N_e is the speed of the engine, M_e is the torque delivered, W_{ip} is the indicated pump work, W_{fr} is the friction work and n_r the number of revolutions

per cycle, equal to two for a four stroke engine. The pumping work is modelled according to (3.10) previously presented in Section 3.2.3:

$$W_{ip}(\theta_{evo}) = (V_{evo}(\theta_{evo}) - V_c) \cdot p_{em} - V_d \cdot p_{im}$$

The friction work can be modelled according to (3.14) as proposed by Heywood [12], which expresses the friction work as a function of the engine speed.

$$W_{fr} = V_D \cdot FMEP(N_e) = V_D \cdot \left(C_{fr,0} + C_{fr,1} \cdot \frac{60N_e}{1000} + C_{fr,2} \cdot \left(\frac{60N_e}{1000} \right)^2 \right) \quad (3.14)$$

With the assumption that the engine speed is constant, the expression in (3.14) is simplified to

$$W_{fr} = V_D \cdot C_{fr} \quad (3.15)$$

where C_{fr} is constant.

3.3.3 Mass flow models

The basis of the air and fuel mass flows modeling is the indicated gross work model presented in (3.16) [23].

$$W_{ig} = m_f \cdot q_{LHV} \cdot \eta_{cycle} \cdot \eta_\lambda \cdot \eta_{ig,ch} \quad (3.16)$$

In (3.16) the product $m_f \cdot q_{LHV}$ represents the total available energy that can be released from the fuel through the combustion process. The factor η_λ represents the efficiency related to the in-cylinder λ-value, and is modelled according to (3.17).

$$\eta_\lambda = \min(1, \lambda) \quad (3.17)$$

In (3.17), η_{cycle} represents the efficiency of the operating cycle, modelled according to the previously presented model in (3.8b):

$$\eta_{cycle} = 1 - \left(\frac{V_{mb50}}{V_{exh}} \right)^{\gamma-1} - \frac{(1 - (A/F)_s \cdot \lambda) \cdot c_v}{q_{LHV}} \cdot \left(\left(\frac{V_c + V_d}{V_{exh}} \right)^{\gamma-1} - 1 \right) \cdot T_{im}$$

The factor $\eta_{ig,ch}$ in (3.16) lumps various losses not captured by η_{cycle}, which arises due to deviations between the real and modelled cycle.

By rearranging (3.16) the expression in (3.18) for fuel mass is obtained.

$$m_f = \frac{W_{ig}}{q_{LHV} \cdot \eta_{cycle} \cdot \eta_\lambda \cdot \eta_{ig,ch}} = \frac{W_{ig}(\theta_{evo})}{q_{LHV} \cdot \eta_{cycle}(\theta_{ig}, \theta_{evo}) \cdot \eta_\lambda \cdot \eta_{ig,ch}} \tag{3.18}$$

Having an expression for the fuel mass, the fuel mass flow can be obtained by using the rotational speed of the engine according to (3.19).

$$\dot{m}_f = \frac{N_e}{n_r} \cdot m_f \tag{3.19}$$

Using the stoichiometric air to fuel ratio and the λ-value, the air mass flow can be determined from the fuel mass flow according to (3.20).

$$\dot{m}_{air} = \left(\frac{A}{F}\right)_s \cdot \lambda \cdot \dot{m}_f \tag{3.20}$$

To obtain the relation between the intake manifold pressure and the air mass flow a model for the volumetric efficiency, η_{vol}, is required. A common approach when modelling the volumetric efficiency is presented in (3.21). This, along with other models for volumetric efficiency, can be found in [23].

$$\dot{m}_{air} = \eta_{vol} \cdot \frac{p_{im} \cdot V_d \cdot n_{cyl} \cdot N_e}{R \cdot T_{im} \cdot n_r} = (c_0 + c_1 \cdot \sqrt{p_{im}} + c_2 \sqrt{N_e}) \cdot \frac{p_{im} \cdot V_d \cdot n_{cyl} \cdot N_e}{R \cdot T_{im} \cdot n_r} \tag{3.21}$$

As for the friction work model, the engine speed can be assumed to be constant within this project. The term related to engine speed in the volumetric efficiency model therefore becomes constant and (3.21) can be simplified to (3.22), where $c_2 \cdot \sqrt{N}$ is included in c_0.

$$\dot{m}_{air} = (c_0 + c_1 \cdot \sqrt{p_{im}}) \cdot \frac{p_{im} \cdot V_d \cdot n_{cyl} \cdot N_e}{R \cdot T_{im} \cdot n_r} \tag{3.22}$$

3.3.4 Heat exchange model

To model the heat losses from the cylinder gas to the surrounding, the initial approach is to consider internal heat transfer from cylinder gas to cylinder wall, and external heat transfer from cylinder wall to the surrounding. The internal heat transfer is modelled as convective heat transfer according to (3.23),

$$\dot{Q}_{ht} = \dot{Q}_{ht,internal} = \dot{Q}_{cyl \to wall} = A_{cyl,in} \cdot h_{cyl,wall} \cdot (T_{cyl} - T_{wall}) \tag{3.23}$$

where $A_{cyl,in}$ is the internal cylinder area, $h_{cyl,wall}$ the heat transfer coefficient, T_{cyl} the cylinder gas temperature and T_{wall} the cylinder wall temperature.

The external heat transfer is assumed to consist of convection and radiation, and is modelled according to (3.24),

$$\begin{aligned}\dot{Q}_{ht,external} = \dot{Q}_{wall\to amb} =& A_{cyl,out} \cdot h_{cyl,wall} \cdot (T_{wall} - T_{amb}) \\ &+ \epsilon \cdot \sigma \cdot A_{cyl,out} \cdot (T_{wall}^4 - T_{amb}^4)\end{aligned} \tag{3.24}$$

where $A_{cyl,out}$ is the outer cylinder area, T_{cyl} the cylinder gas temperature, ϵ the emissivity coefficient and σ the Stefan–Boltzmann constant. The temperature dynamics of the cylinder wall can be described using energy balance where the temperature change is driven by the difference $\dot{Q}_{ht,external} - \dot{Q}_{ht,internal}$, according to (3.25)

$$\frac{dT_{wall}}{dt} \cdot m_{wall} \cdot c_{wall} = \dot{Q}_{cyl\to wall} - \dot{Q}_{wall\to amb} \tag{3.25}$$

where m_{wall} is the wall mass and c_{wall} specific heat capacity.

Within this project measurement data for the in-cylinder temperature T_{cyl} and the cylinder wall temperature T_{wall} are not available, and some modifications to the presented model are therefore necessary. The temperature dynamics of the cylinder wall are not modelled, and the wall temperature is instead modelled as proportional to the engine out temperature according to (3.26).

$$T_{wall} = k_{ht} \cdot T_{eo} \tag{3.26}$$

By using the assumption that the wall temperature is proportional to the engine out temperature, the cylinder heat losses can be modelled as only the external heat transfer presented in (3.24), and measurements for the in-cylinder temperature is not necessary. The heat transfer can now be modelled according to (3.27).

$$\begin{aligned}\dot{Q}_{ht} &= A_{cyl,out} \cdot h_{cyl,wall} \cdot (T_{wall} - T_{amb}) + \epsilon \cdot \sigma \cdot A_{cyl,out} \cdot (T_{wall}^4 - T_{amb}^4) \\ &= A_{cyl,out} \cdot h_{cyl,wall} \cdot (k_{ht} \cdot T_{eo} - T_{amb}) + \epsilon \cdot \sigma \cdot A_{cyl,out} \cdot ({k_{ht}}^4 \cdot T_{eo}^4 - T_{amb}^4)\end{aligned} \tag{3.27}$$

Since the expression for heat exchange in (3.27) is to be inserted into the cylinder-out temperature model in (3.12) and be solved for T_{eo}, a forth order expression is undesirable. The terms related to heat losses due to radiation is therefore linearized, resulting in the expression in (3.28).

$$\dot{Q}_{ht} = A_{cyl,out} \cdot h_{cyl,wall} \cdot (k_{ht} \cdot T_{eo} - T_{amb}) + \epsilon \cdot \sigma \cdot A_{cyl,out} \cdot (k_{ht} \cdot T_{eo} - T_{amb}) \tag{3.28}$$

By lumping the constant parameters in (3.28) the simple affine function of T_{eo} presented in (3.29) can be used to model the cylinder heat exchange.

$$\dot{Q}_{ht} = c_{ht,1} + c_{ht,2} \cdot T_{eo} \tag{3.29}$$

By inserting (3.29) into (3.12) the engine out-temperature T_{eo} can be expressed according to (3.30).

$$T_{eo} = \frac{\dot{m}_{air} c_p T_{im} + \dot{m}_f c_p T_f + \dot{m}_f q_{LHV} \eta_\lambda - x_e \dot{m}_f h_{fg} - W_{ig} - c_{ht,1}}{c_p(\dot{m}_{air} + \dot{m}_f) + c_{ht,2}} \tag{3.30}$$

The expression in (3.30) is the proposed engine out-temperature model.

3.3.5 Cylinder model summary

A summary of the proposed model for the cylinder-out temperature is presented below.

Proposed cylinder out-temperature model

$$T_{eo} = \frac{\dot{m}_{air} c_p T_{im} + \dot{m}_f c_p T_f + \dot{m}_f q_{LHV} \eta_\lambda - x_e \dot{m}_f h_{fg} - \dot{W}_{ig} - \dot{Q}_{ht}}{c_p(\dot{m}_{air} + \dot{m}_f)}$$

$$\dot{W}_{ig}(\theta_{evo}) = \frac{N_e}{n_r} \cdot \left(2\pi n_r M_e + W_{ip}(\theta_{evo}) + W_{fr}\right)$$

$$W_{ip}(\theta_{evo}) = (V_{evo}(\theta_{evo}) - V_c) \cdot p_{em} - V_d \cdot p_{im}$$

$$W_{fr} = V_D \cdot C_{fr}$$

$$\dot{m}_f(\theta_{MB50}, \theta_{evo}) = \frac{N_e}{n_r} \cdot \frac{W_{ig}(\theta_{evo})}{q_{LHV} \cdot \eta_{cycle}(\theta_{MB50}, \theta_{evo}) \cdot \eta_\lambda \cdot \eta_{ig,ch}}$$

$$\eta_{cycle}(\theta_{ig}, \theta_{evo}) = 1 - \left(\frac{V_{MB50}(\theta_{ig})}{V_{evo}(\theta_{evo})}\right)^{\gamma-1} - \frac{(1 - (A/F)_s \cdot \lambda) \cdot c_v}{q_{LHV}} \cdot \left(\left(\frac{V_c + V_d}{V_{evo}(\theta_{evo})}\right)^{\gamma-1} - 1\right) \cdot T_{im}$$

$$\eta_\lambda = \min(1, \lambda)$$

$$\dot{m}_{air} = \left(\frac{A}{F}\right)_s \cdot \lambda \cdot \dot{m}_f$$

$$\dot{m}_{air} = (c_0 + c_1 \cdot \sqrt{p_{im}}) \cdot \frac{p_{im} \cdot V_d \cdot n_{cyl} \cdot N_e}{R \cdot T_{im} \cdot n_r}$$

$$\dot{Q}_{ht} = c_{ht,1} + c_{ht,2} \cdot T_{eo}$$

$$V_{MB50}(\Delta\theta_{ig}) = V_d \cdot \left(\frac{1}{r_c - 1} + \frac{1}{2} \cdot \left(\frac{l}{a} + 1 - cos(c_{ig,1} + c_{ig,2} \cdot \Delta\theta_{ig}) - \sqrt{\left(\frac{l}{a}\right)^2 - sin^2(c_{ig,1} + c_{ig,2} \cdot \Delta\theta_{ig})}\right)\right)$$

$$V_{evo}(\Delta\theta_{evo}) = V_d \cdot \left(\frac{1}{r_c - 1} + \frac{1}{2} \cdot \left(\frac{l}{a} + 1 - cos(c_{evo,1} + c_{evo,2} \cdot \Delta\theta_{evo}) - \sqrt{\left(\frac{l}{a}\right)^2 - sin^2(c_{evo,1} + c_{evo,2} \cdot \Delta\theta_{evo})}\right)\right)$$

$$\theta_{MB50} = c_{ig,1} + c_{ig,2} \cdot \Delta\theta_{ig}$$

$$\theta_{evo} = c_{evo,1} + c_{evo,2} \cdot \Delta\theta_{evo}$$

By observing the proposed cylinder model some conclusions can be drawn regarding the effect on engine out-temperature caused by variations in ignition and exhaust valve opening angles. The ignition angle, θ_{ig}, and the exhaust valve opening angle, θ_{evo}, are directly affecting the cylinder volumes V_{MB50} and V_{evo}, which

in turn affects the cycle efficiency η_{cycle} and the pumping work W_{ip}. The variations in cycle efficiency and pumping work will cause variations in fuel and air mass flows, $\dot{m}_f$ and $\dot{m}_{air}$, and engine power $\dot{W}_{ig}$. These variations will directly affect the engine out temperature T_{eo}.

3.4 Temperature dynamics in exhaust manifold

In order to obtain a model which captures the dynamic behaviour of the temperature in the exhaust manifold a first order time dynamic is introduced. The dynamic is introduced through (3.31) which models the temperature T_{em} in the exhaust manifold.

$$\frac{dT_{em}}{dt} = \frac{1}{\tau_{em}} \cdot (T_{eo} - T_{em}) \tag{3.31}$$

In (3.31) the parameter τ_{em} is the time constant of the first order system. The dynamic behaviour of the exhaust manifold temperature can be further modelled by also introducing a time delay. However, such a time delay is believed to be small enough to be neglected.

3.5 Turbine model

3.5.1 Turbine temperature loss model

The modelling of the turbine is based on the static model in (3.32), which has been validated to give good accuracy to measured data in, for example, [27]. In (3.32), T_{em} is the exhaust temperature on the inlet side of the turbine, $T_{t,out}$ the temperature on the outlet side, T_g the temperature of the gas inside the turbine, $T_{t,sol}$ the temperature of the turbine housing and $\dot{m}_{exh,t}$ the exhaust mass flow through the turbine.

$$\dot{m}_{exh,t} c_{p,exh} (T_{em} - T_{t,out}) = h_{t,in} A_{t,in} (T_g - T_{t,sol}) + \dot{W}_t \tag{3.32}$$

The model (3.32) is based on the first law of thermodynamics and contains the enthalpy change of the exhaust gases on the left hand side. On the right hand side the first term represents the heat transfer from the exhaust gases to the turbine housing, and the second term represents the power produced by the turbine. In (3.32) it is assumed that the convection from exhaust gas to turbine housing is assumed to occur with uniform temperature, although in reality there is a temperature drop over the turbine. The temperature inside the turbine, T_g, requires some modelling since it is not possible to measure with the experimental setup used within this project. Many different models can be proposed for this temperature, but in this project it is modelled as the mean value of the inlet and outlet temperatures of the turbine, according to (3.33).

$$T_g = \frac{T_{t,out} + T_{em}}{2} \tag{3.33}$$

The power produced by the turbine is modelled as the sum of the compressor power and the power required to overcome friction. However, it is assumed that $\dot{W}_c >> \dot{W}_{fric}$ and the turbine power can therefore be modelled according to (3.34),

$$\dot{W}_t = \dot{W}_c + \dot{W}_{fric} \approx \dot{W}_c = \dot{m}_{air} c_{p,air} (T_{c,out} - T_{c,in}) \tag{3.34}$$

where $\dot{m}_{air}$ is the air mass flow though the compressor. By modelling the turbine power according to (3.34) not only are the friction losses ignored but also some heat exchange which occur at the compressor. These are however considered to be negligible.

The temperature dynamics of the turbine housing temperature, $T_{t,sol}$, can be described according to (3.35),

$$\begin{aligned} \frac{dT_{t,sol}}{dt} m_{t,sol} c_{t,sol} = {} & h_{t,in} A_{t,in} (T_g - T_{t,sol}) - h_{t,out} A_{t,out} (T_{t,sol} - T_{amb}) \\ & - \epsilon \sigma A_{t,out} (T_{t,sol}^4 - T_{amb}^4) \end{aligned} \tag{3.35}$$

where $m_{t,sol}$ is the solid mass of the turbine and $c_{t,sol}$ the specific heat capacity. The first term on the right hand side in (3.35) represents the convection from turbine gas to turbine housing, and the second and third terms represents the convection and radiation from turbine housing to the surrounding, which is assumed to be of ambient temperature. As for the cylinder heat exchange model, this dynamic temperature model causes issues since the experimental setup used does not allow measuring of the turbine housing temperature. To work around this issue, the turbine housing temperature is modelled as proportional to the outlet temperature of the turbine, $T_{t,out}$, according to (3.36)

$$T_{t,sol} = c_{t,1} \cdot T_{t,out} \tag{3.36}$$

Inserting (3.36) together with (3.33) and (3.34) into (3.32) the turbine outlet temperature can be modelled according to (3.37).

$$T_{t,out} = \frac{\left(\dot{m}_{exh,t} \cdot c_{p,exh} - \frac{h_{t,in} \cdot A_{t,in}}{2} \right) \cdot T_{em} - \dot{m}_{air} \cdot c_{p,air} \cdot (T_{c,out} - T_{c,in})}{\dot{m}_{exh,t} \cdot c_{p,exh} + \frac{h_{t,in} \cdot A_{t,in}}{2} - c_{t,1}} \tag{3.37}$$

By introducing the lumped parameter $c_{t,2} = \frac{h_{t,in} \cdot A_{t,in}}{2}$, (3.37) becomes (3.38).

$$T_{t,out} = \frac{\left(\dot{m}_{exh,t} \cdot c_{p,exh} - c_{t,2}\right) \cdot T_{em} - \dot{m}_{air} \cdot c_{p,air} \cdot (T_{c,out} - T_{c,in})}{\dot{m}_{exh,t} \cdot c_{p,exh} + c_{t,2} - c_{t,1}} \tag{3.38}$$

Finally, the compressor inlet temperature is assumed to be ambient, $T_{c,in} = T_{amb}$, and the compressor outlet temperature a linear function of turbine mass flow, according to (3.39).

$$T_{c,out} = c_{comp,0} + c_{comp,1} \cdot \dot{m}_{exh,t} \tag{3.39}$$

3.5.2 Wastegate loss model

To model the temperature losses of the exhaust gas through the wastegate, the model presented in (3.40) is proposed, which can be found in [7].

$$T_{wg,out} = T_{amb} + (T_{em} - T_{amb}) e^{\frac{-h_{tot} A}{\dot{m}_{exh,wg} \cdot c_{p,exh}}} \tag{3.40}$$

In (3.40) the temperature T_{amb} is the temperature of the surrounding, which is assumed to be ambient. T_{em} is the temperature in the exhaust manifold and $\dot{m}_{exh,wg}$ is the exhasut mass flow through the wastegate. h_{tot} is the total heat transfer coefficient between the wastegate inlet and outlet, where heat transfer due to convection, conducting and radiation is included. By lumping the constants in the exponent of (3.40) into one constant, c_{wg}, the expression in (3.41) is obtained, which is the model initially used to model the wastegate heat losses.

$$T_{wg,out} = T_{amb} + (T_{em} - T_{amb}) e^{\frac{-c_{wg}}{\dot{m}_{exh,wg}}} \tag{3.41}$$

In a second iteration, the constant c_{wg} was replaced by a first order polynomial where the wastegate mass flow is included, changing the model according to (3.42).

$$T_{wg,out} = T_{amb} + (T_{em} - T_{amb}) e^{-\frac{c_{wg,1} + c_{wg,2} \cdot \dot{m}_{exh,wg}}{\dot{m}_{exh,wg}}} \tag{3.42}$$

This change was introduced in order to make the model fit measurement data more accurately, and is further motivated by the model validation presented in Chapter 6. A possible reason why the polynomial expression gives an improved fit to measurement data is that the value of h_{tot} is likely to vary with varied mass flow due to the effect of forced convection.

3.5.3 Temperature after turbine

The temperature of the exhaust gases after the turbine is dependant of the temperature of the gases through the turbine, and the temperature of the gases through the wastegate. The temperature and mass flow relations presented in (3.43) is used as the model for exhaust gas tempereature after the turbine and wastegate.

$$T_{at} = \frac{T_{t,out} \cdot \dot{m}_{exh,t} + T_{wg,out} \cdot \dot{m}_{exh,wg}}{\dot{m}_{exh,t} + \dot{m}_{exh,wg}} \tag{3.43}$$

3.6 Pipe loss model

3.6.1 Stationary heat losses

To accurately model the temperature of the exhaust gas at the catalytic converter inlet, a model which considers temperature losses in the pipe section between the turbine and the catalytic converter is required. A proposed model is presented in (3.44), which can be found in [7] and is the same model as used for the wastegate temperature losses in (3.40).

$$T_{pipe,end} = T_{amb} + (T_{at} - T_{amb}) e^{\frac{-h_{tot} A}{\dot{m}_{exh} \cdot c_{p,exh}}} \tag{3.44}$$

By lumping the constant parameters in the exponent of (3.44) into one parameter in the same manner as for the wastegate model, the expression in (3.45) is obtained.

$$T_{pipe,end} = T_{amb} + (T_{at} - T_{amb}) e^{\frac{-c_{pipe}}{\dot{m}_{exh}}} \tag{3.45}$$

As for the wastegate model, the constant c_{pipe} was replaced with a polynomial in the second iteration in order to fit measurement data more accurately. The model is thus changed according to (3.46).

$$T_{pipe,end} = T_{amb} + (T_{at} - T_{amb}) e^{-\frac{c_{pipe,1} + c_{pipe,2} \cdot \dot{m}_{exh}}{\dot{m}_{exh}}} \tag{3.46}$$

3.6.2 Pipe temperature dynamics

For the pipe section between the turbine outlet and catalytic converter inlet some temperature dynamics are introduced in the model. As for the exhaust manifold model, a first order time constant is introduced through (3.47) which models the catalytic converter inlet temperature $T_{cat,in}$.

$$\frac{d T_{cat,in}}{dt} = \frac{1}{\tau_{pipe}} \cdot (T_{pipe,end} - T_{cat,in}) \tag{3.47}$$

3.7 Catalytic converter temperature model

The catalytic converter temperature model used within this project originates from [13], and is presented in equation (3.48).

$$\frac{dT_{cat,out}}{dt} = -\frac{4 \cdot \dot{m}_{exh} \cdot c_{p,exh}}{L \cdot (1-\epsilon) \cdot \rho_s c_{p,s} \pi D^2}(T_{cat,out} - T_{cat,in}) \tag{3.48}$$

When modelling the temperature of the catalytic converter according to (3.48) some assumptions are made [13]. Instant temperature equilibrium between the exhaust gas and the catalyst substrate is assumed, as well as no heat conduction in the catalyst substrate. Furthermore, no chemical reactions are modelled which makes the proposed model a very simplified catalytic converter model. However, since only the temperature of the catalytic converter is of interest within this project it is believed that a simple model is sufficient, given it can provide a sufficient estimation of the catalytic converter temperature given a certain inlet exhaust gas temperature.

The catalytic converter temperature model presented in (3.48) can be extended to represent the catalytic converter divided into N segments, according to (3.49).

$$\frac{dT}{dt} = -\frac{4 \cdot N \cdot \dot{m}_{exh} \cdot c_{p,exh}}{L \cdot (1-\epsilon) \cdot \rho_s c_{p,s} \pi D^2}(AT + BT_{cat,in}) \tag{3.49}$$

In (3.49), T is a vector with N elements, and the *i:th* element is the temperature of segment i. The parameters A and B represent the following matrices:

$$A = \begin{pmatrix} -1 & 0 & 0 & \dots & 0 \\ 1 & -1 & 0 & \dots & 0 \\ 0 & 1 & -1 & \dots & 0 \\ \vdots & \vdots & \ddots & \ddots & \vdots \\ 0 & 0 & \dots & 1 & -1 \end{pmatrix}, \qquad B = \begin{pmatrix} 1 \\ 0 \\ 0 \\ \vdots \\ 0 \end{pmatrix}$$

By further introducing the lumped parameter $M = -\frac{4N c_{p,exh}}{L \cdot (1-\epsilon) \cdot \rho_s c_{p,s} \pi D^2}$ the model in (3.49) can be simplified to (3.50).

$$\frac{dT}{dt} = \dot{m}_{exh} \cdot M \cdot (AT + BT_{cat,in}) \tag{3.50}$$

Using this model only one parameter, M, is left to be estimated to obtain a model which fit to measured data.

4

Optimal control

4.1 Formulation of optimal control problems

In order to be able to analyze the optimal control strategy for the catalytic converter heating process, it is necessary to formulate an optimal control problem, OCP. A typical way to set up an OCP is to formulate it as an optimization problem according to (4.1).

$$\underset{x,u}{\text{minimize}} \quad \psi(x(T)) + \int_0^T L(x(t), u(t))dt \tag{4.1}$$

$$\text{subject to} \quad x(0) = x_0 \tag{4.2}$$

$$x(T) = x_T \tag{4.3}$$

$$\dot{x}(t) = f(t, x(t), u(t)) \tag{4.4}$$

In (4.1) $x(t)$ are the states at time t, and $u(t)$ are the controls at time t. The first term in (4.1) is the terminal state cost and $L(x(t), u(t))$ in the second term is the Lagrange term. In the first constraint (4.2), x_0 is the initial state values and in the second constraint (4.3), x_T is the state values at the final time T. In the third constraint (4.4), $\dot{x}(t)$ is the state derivative with respect to time and $f(t, x(t), u(t))$ is the differential equations describing the system dynamics.

4.2 Numerical solutions to optimal control problems

For solving of optimal control problems there are three different families of methods that can be used; *dynamic programming*, *indirect methods* and *direct methods*.

The basis of dynamic programming is solving the *Hamilton-Jacobi-Bellman* (*HJB*) equation. Some disadvantages of dynamic programming are that the value function has to be continuously differentiable, and the so-called "*curse of dimensionability*" which means that the numerical solution becomes very expensive in larger state dimensions. When applying dynamic programming to time discrete problems the "*curse of dimensionability*" is still an issue which limits the methods practical applicability to systems with no more than $n_x \approx 6$ number of states [6].

The indirect methods are based on *Pontryagin's Maximum Principle* (*PMP*) which descibes the necessary optimality conditions for optimal control in continuous time. These conditions are used to eliminate the controls from the problem and numerically solving a boundary value problem. Some drawbacks of the indirect methods are, for example, that the controls must be able to be eliminated from the problem algebraically, and that the optimal controls might be discontinuous functions of x [6].

The direct methods discretize the optimal control problem into a *nonlinear program* (*NLP*), which can be solved using various different *NLP* solution methods. The direct methods can therefore be described as "*First discretize, then optimize*". Common methods to solve the *NLP* are *direct single shooting*, *direct multiple shooting* and *direct collacation* [6].

The intention of this section is to only present a brief overview of the methods to find the numerical solutions to optimal control problems. For more in-depth presentations the reader is referred to other documentation regarding the different methods.

4.3 Optimizations using CasADi

In order to investigate the optimal control strategy for catalytic converter heating, CasADi [3] is used together with Matlab to solve optimal control problems within this project. Although CasADi is not explicitly a tool for solving OPCs, it is a useful software tool providing building blocks that allows the user to implement and solve OPCs. No more in-depth details will be presented regarding how CasADi works, and the reader is referred to the dissertation [3] for further reading.

4.3.1 Direct multiple shooting

The chosen method used for solving the OPCs in this project is a *direct method*, and more specifically *direct multiple shooting*. As was stated in section (4.2) the direct methods are based on the idea of converting the OCP into a NLP, which is performed by discretizing the independent variable, in this case time. If the time interval $t \in [0, T]$ is divided into N segments of equal length, the length of each segment is h according to (4.5).

$$h = \frac{T}{N} \tag{4.5}$$

For each control interval the control signal u are set as constant according to (4.6),

$$u(t) = q_i \tag{4.6}$$

where:

$$\begin{aligned} &t \in [t_i, t_{i+1}], \quad i = 0, ..., N-1 \\ &t_{i+1} = t_i + h \\ &t_0 = 0 \\ &t_N = T \end{aligned}$$

Making the control signals piecewise constant over the total time interval, the state trajectory for each segment is numerically computed according to (4.7),

$$x(t_{i+1}) = F(t_i, x_i, u_i) \approx \int_{t_i}^{t_{i+1}} f(t, x(t), u(t))dt \tag{4.7}$$

where $F(t, x, u)$ is the numerical integration method. Likewise, the cost of each segment is also calculated using numerical integration according to (4.8).

$$l_i(t_i, x_i, u_i) = \int_{t_i}^{t_{i+1}} L(t, x(t), u(t))dt \tag{4.8}$$

Since the system is integrated separately on each time interval in (4.7), the obtained state trajectory is not continuous. The constraint in (4.9) is therefore introduced with the purpose of joining each segment with the previous one.

$$x_{i+1} - F(t_i, x_i, u_i) = 0 \quad \text{for} \quad i = 0, ...N-1 \tag{4.9}$$

Combining (4.5) - (4.9) the OCP can now be formulated as a NLP given by (4.10) - (4.14).

$$\underset{u}{\text{minimize}} \quad \sum_{i=0}^{N-1} l_i(t_i, x_i, u_i) + E(T, x_N) \tag{4.10}$$

$$\begin{aligned} \text{subject to} \quad & x(0) = x_0 && (4.11)\\ & x(T) = x_T && (4.12)\\ & h(x_i, u_i) \leq 0, \quad i = 0, ..., N && (4.13)\\ & x_{i+1} - F(t_i, x_i, u_i) = 0, \quad i = 0, ..., N && (4.14) \end{aligned}$$

The constraints in (4.11) and (4.12) are the initial and final state values as in (4.2) and (4.3). In (4.13) the discretized path constraints are defined and (4.14) is the continuity constraint.

4.3.2 Fourth Order Runge-Kutta Method

The numerical integration method used in this project is the *fourth order Runge-Kutta method*, sometimes also referred to as *classical Runge-Kutta method* or just *the Runge-Kutta method*. Using this numerical integration method the state values x_{i+1} at time $t = i + 1$ are calculated using the state values x_i and control signals u_i at time $t = i$, according to (4.15)

$$x_{i+1} = x_n + \frac{h}{6} \cdot (k_1 + 2 \cdot k_2 + 2 \cdot k_3 + k_4) \tag{4.15}$$

where h is defined according to (4.5). With a function $f(x, u)$ which describes the system dynamics according to (4.16)

$$\dot{x} = f(x(t), u(t)) \tag{4.16}$$

the slope approximations are given by (4.17).

$$\begin{cases} k_1 = f(x_i, u_i) \\ k_2 = f(x_i + k_1 \cdot \frac{h}{2}, u_i) \\ k_3 = f(x_i + k_2 \cdot \frac{h}{2}, u_i) \\ k_4 = f(x_i + k_3 \cdot h, u_i) \end{cases} \tag{4.17}$$

It should be highlighted that in (4.17) the control signals u_i are constant for the entire time step as presented in section 4.3.1. In words, the fourth order Runge-Kutta method estimates the slope at the start of the time step, k_1, the midpoint of the step, k_2 and k_3, and at the end point of the step, k_4. The estimation of x_{i+1} is then made through the use of the weighted sum of these slopes.

4.3.3 Performed optimizations

Variations in $\Delta\theta_{ig}$ and $\Delta\theta_{evo}$

Optimization were performed using the models presented in chapter 3 and the time discretization presented in section 4.3.1. The optimal control strategies were studied for two different cases; wastegate fully opened and wastegate fully closed. Each optimization was performed with the time interval divided into $N = 500$ segments. Also, all optimizations were performed with the constraints that the initial temperatures in exhaust manifold, at catalyst inlet and at catalyst outlet are ambient and the final temperature at the catalyst outlet is 550 K. The variations in ignition and exhaust valve opening angles are the control signals and are

varied within the intervals $0 \leq \Delta\theta_{ig} \leq 12$ and $0 \leq \Delta\theta_{evo} \leq 30$, expressed in CAD.

Two different types of optimizations were performed for each case. In the first optimization the system is optimized to achieve the shortest heating time for the catalytic converter. For this case, the optimization problem can be formulated according to,

$$\begin{aligned} \underset{x,u}{\text{minimize}} \quad & \int_0^T dt \\ \text{subject to} \quad & T_{em}(0) = T_{amb} \\ & T_{cat,in}(0) = T_{amb} \\ & T_{cat,out}(0) = T_{amb} \\ & T_{cat,out}(T) = 550 \text{ K} \\ & N_e = 1500 \text{ RPM} \\ & M_e = 90 \text{ Nm} \\ & 0 \leq \Delta\theta_{ig} \leq 12 \\ & 0 \leq \Delta\theta_{evo} \leq 30 \\ & \dot{x}(t) = f(t, x(t), u(t)) \end{aligned} \tag{4.18}$$

where $f(t, x(t), u(t))$ represents the models presented in chapter 3.

The second optimization is performed to obtain the lowest accumulated fuel consumption required to reach $T_{cat,out} = 550$ K for a fixed final time value T. For this case the optimization problem can be formulated according to,

$$\begin{aligned} \underset{x,u}{\text{minimize}} \quad & \int_0^T \dot{m}_f dt \\ \text{subject to} \quad & T_{em}(0) = T_{amb} \\ & T_{cat,in}(0) = T_{amb} \\ & T_{cat,out}(0) = T_{amb} \\ & T_{cat,out}(T) = 550 \text{ K} \\ & N_e = 1500 \text{ RPM} \\ & M_e = 90 \text{ Nm} \\ & 0 \leq \Delta\theta_{ig} \leq 12 \\ & 0 \leq \Delta\theta_{evo} \leq 30 \\ & \dot{x}(t) = f(t, x(t), u(t)) \end{aligned} \tag{4.19}$$

where $\dot{m}_f$ is modelled according to chapter 3.

Before the optimizations presented above were performed the full model was simulated with $\Delta\theta_{ig} = 0$, $\Delta\theta_{evo} = 0$ and $\lambda = 1$ to obtain reference values for catalytic converter heating time and fuel consumption.

Variations in $\Delta\theta_{ig}$, $\Delta\theta_{evo}$ and λ

In addition to the optimizations with variable θ_{ig} and θ_{evo}, additional optimizations were also performed with variable λ within the interval $1 \leq \lambda \leq 1.2$. With λ as an additional control signal the performed optimizations are the same as presented in (4.18) and (4.19), with $1 \leq \lambda \leq 1.2$ added as new constraint to the NLPs.

5

Measurements

Measurements were performed on a test engine at the division of Vehicular Systems, Linköping University. The purpose of the measurements was to obtain data to validate the models presented in chapter 3. The measurements can be divided into two different types, stationary measurements and dynamic measurements.

5.1 Stationary measurements

The stationary measurements were performed at one speed-torque operating point at which the ignition and exhaust valve opening angles were varied. The stationary measurements are divided into two different cases; fully open wastegate and fully closed wastegate. For the two cases measurements were conducted for different ignition and exhaust valve opening angles, as presented in Tables 5.1 and 5.2. As defined in (3.2), positive values for $\Delta\theta_{ig}$ and $\Delta\theta_{evo}$ respresents deviations closer to TDC. The stationary measurements were performed at $M_e = 90$ Nm and $N_e = 1500$ rpm.

Table 5.1: *Data collection points for the stationary measurements at $M_e = 90$ Nm and $N = 1500$ rpm with fully open wastegate.*

$\Delta\theta_{ig}$ \ $\Delta\theta_{evo}$	0 [CAD]	10.0 [CAD]	20.0 [CAD]	30.0 [CAD]
0.0 [CAD]	X	X	X	X
4.0 [CAD]	X			X
8.0 [CAD]	X			X
12.0 [CAD]	X	X	X	

Table 5.2: *Data collection points for the stationary measurements at M_e = 90 Nm and N = 1500 rpm with fully closed wastegate.*

$\Delta\theta_{ig}$ \ $\Delta\theta_{evo}$	0 [CAD]	15.0 [CAD]	30.0 [CAD]
0.0 [CAD]	X		X
6.0 [CAD]		X	
12.0 [CAD]	X		X

The purpose of the stationary measurements is to obtain data which can be used to estimate the unknown parameters in the stationary models presented in chapter 3.

5.2 Dynamic measurements

Dynamic measurement were performed in order to obtain data which can be analyzed to obtain better understanding of the dynamic behaviour of the temperatures in the exhaust system. The dynamic measurements consists of the following:

- Data collection during engine cold start with closed wastegate
- Data collection during a step in ignition angle from $\Delta\theta_{ig}$ = 0 [CAD] to $\Delta\theta_{ig}$ = 12 [CAD] with wastegate fully closed
- Data collection during a step in ignition angle from $\Delta\theta_{ig}$ = 0 [CAD] to $\Delta\theta_{ig}$ = 12 [CAD] with wastegate fully open

The cold start measurements were performed at the operating point N_e = 875 RPM and M_e = 0 Nm, and the ignition step measurements at N_e = 1500 RPM and M_e = 90 Nm.

The purpose of the cold start measurement is primarily to gather data to be used for the catalytic converter temperature model. The purpose of performing measurements for a step in ignition angle is to obtain data during dynamic temperature behaviour, since such a step will affect the engine out-temperature. The collected data is then to be used to estimate the dynamic time constants in the exhaust manifold and pipe section between turbine outlet and catalytic converter inlet, as presented in chapter 3.

5.3 Measured data

During the measurements, data were collection for the quantities presented in Table 5.3.

Table 5.3: *Summary of the measured quantities.*

Quantity	Notation	Description
Mass flow	$\dot{m}_{air}$	Air mass flow [kg s^{-1}]
Temperatures	T_{im}	Intake manifold temperature [K]
	T_{eo}	Cylinder-out temperature [K]
	$T_{t,out}$	Turbine outlet temperature [K]
	$T_{cat,in}$	Catalyst intake temperature [K]
	$T_{cat,out}$	Catalyst outlet temperature [K]
	T_{amb}	Surrounding ambient temperature [K]
	$T_{c,in}$	Compressor intake temperature [K]
	$T_{c,out}$	Compressor outlet temperature [K]
Pressures	p_{im}	Intake manifold pressure [Pa]
	p_{em}	Exhaust manifold pressure [Pa]
	p_{at}	Pressure after turbine [Pa]
Other	λ	Lambda value [-]

5.4 Measurement uncertainties

Within this project some uncertainties arise which are related to the measurements performed on the test engine. For the stationary measurements some uncertainties are present due to the fact that the measurements presented in Tables 5.1 and 5.2 were performed at two separate sessions. Between the first session, where the data in Table 5.1 were collected, and the second session, where the data in Table 5.2 were collected, the test engine had been both dissembled and reassembled, possibly affecting some of the engine properties. In addition to

this there is a potential risk that some leakage of exhaust gases were present due to the engine being equipped with old manifold packing at the time of the second measurement session. Combining the dissembling and reassembling of the engine with the potential exhaust gas leakage, there is a risk that the engine properties have been different at the two measurement sessions which can affect the outcome of the estimation and validation of the models.

Another uncertainty, primarily affecting the dynamic measurements, is that the temperature sensor positioned at the turbine outlet is positioned in such a way that when the wastegate is open it is not well positioned in the mass flow. For the dynamic step measurement with open wastegate, the data for the turbine outlet temperature is therefore possibly too unreliable to be used for the estimation of the pipe time constant. This seems to be an issue primarily for the dynamic measurements when the dynamic temperature changes are not properly captured in the measurement data.

6

Model validation

Based on the collected measurement data, the model parameters in the models presented in Chapter 3 were estimated. In this chapter the models for engine out temperature, turbine outlet temperature, wastegate outlet temperature, pipe loss temperature, catalyst inlet temperature, catalyst outlet temperature and air mass flow are validated by comparison to data collected in the engine test stand. The models for temperature dynamics in the exhaust manifold and pipe section between turbine outlet and catalyst inlet are also validated.

As presented in Section 5.4 some potential exhaust gas leakage was present during the data collection with closed wastegate. Because of this, the measurement data collected with closed wastegate, Table 5.2, is only used for estimation and validation of the turbine model, and all other models are estimated using only the open wastegate measurement data, Table 5.1. This is to ensure that model errors due to potential leakage is minimized.

6.1 Mass flow model

The estimated and measured air mass flows are presented in Figure 6.1. The mean average error (*MAE*) for the mass flow model is $8.3 \cdot 10^{-5}$ kg/s, equivalent to 0.48%.

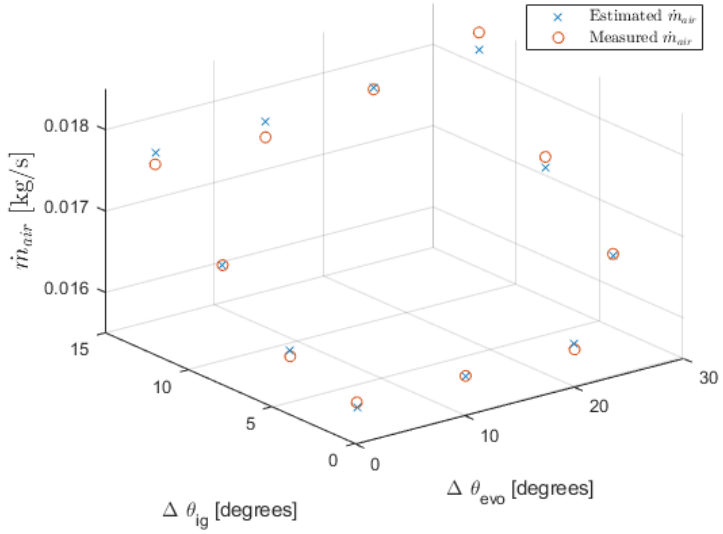

(a) *A 3D visualisation of the estimated and measured air mass flows at statioary conditions.*

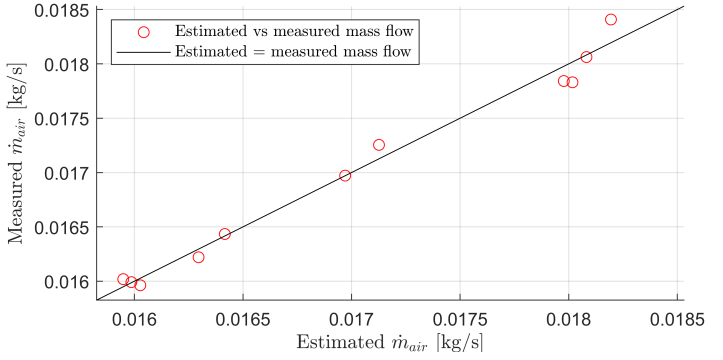

(b) *The measured air mass flows at plotted against the estimated values at stationary conditions.*

Figure 6.1: *Visual comparisons between the measured and estimated air mass flows.*

6.2 Engine out temperature

The estimated and measured engine out temperatures are presented in Figure 6.2. The MAE for the cylinder out temperature model is 3.35 K, or 0.35%.

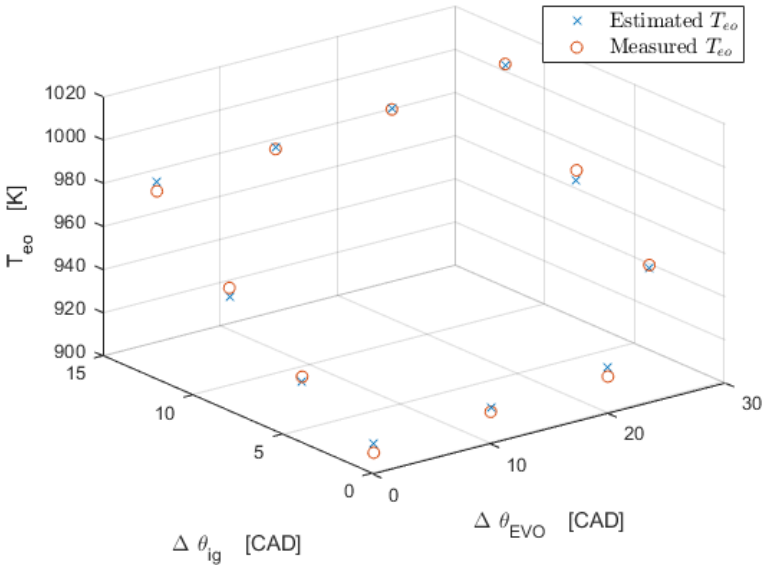

(a) *A 3D visualisation of the estimated and measured engine out temperature at stationary conditions.*

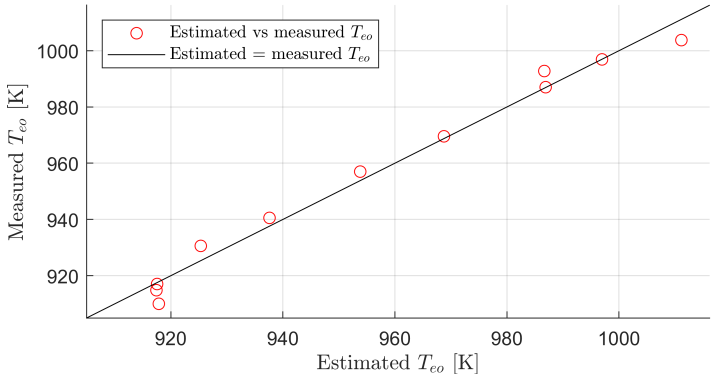

(b) *The measured engine out temperature plotted against the estimated values at stationary conditions.*

Figure 6.2: *Visual comparisons between the measured and estimated engine out temperatures.*

6.3 Turbine temperature loss model

The estimated and measured temperatures after turbine is presented in Figure 6.3. The MAE for the turbine outlet temperature model is 3.93 K, or 0.41%.

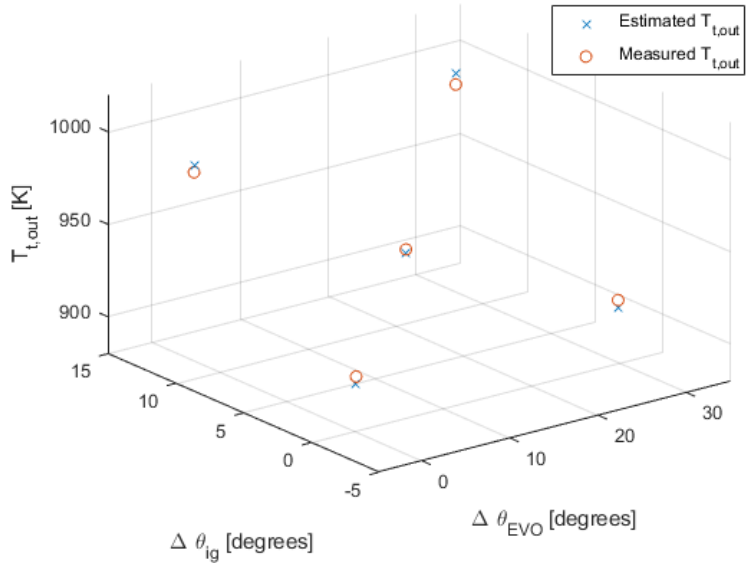

(a) *A 3D visualization of the estimated and measured turbine outlet temperatures.*

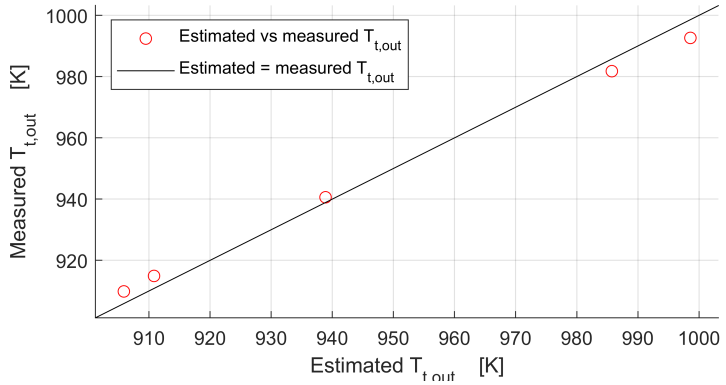

(b) *The measured turbine outlet temperatures plotted against the estimated values at stationary conditions.*

Figure 6.3: *Visual comparisons between the measured and estimated turbine outlet temperatures at stationary conditions.*

6.4 Wastegate temperature model

The estimated and measured wastegate out temperatures are presented in Figure 6.4 for the initial wastegate model, presented in (3.41).

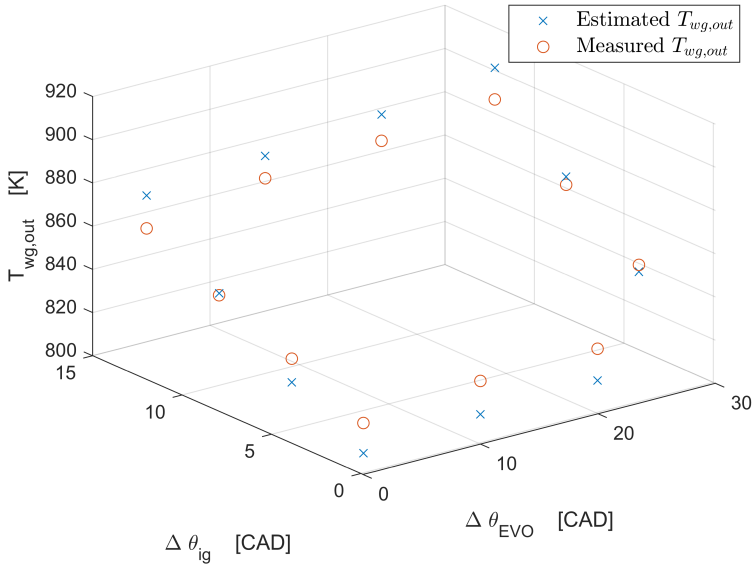

(a) *A 3D visualisation of the estimated and measured $T_{wg,out}$ at stationary conditions using the initial model.*

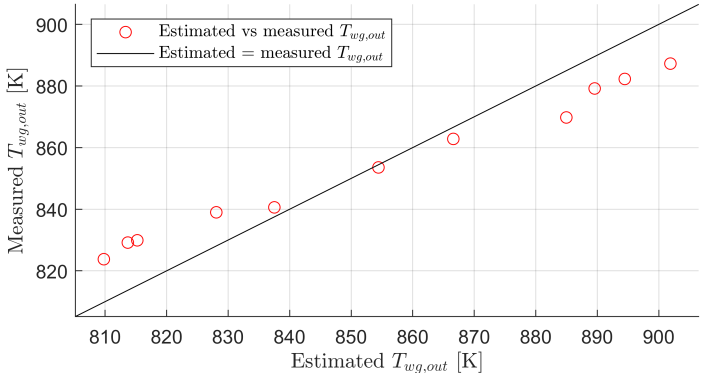

(b) *The measured $T_{wg,out}$ plotted against the estimated values at stationary conditions using the initial model.*

Figure 6.4: *Visual comparisons between the measured and estimated wastegate out temperatures using the initial model.*

The MAE for the wastegate temperature validated in Figure 6.4 is 10.47 K, or

1.23%. The temperature estimated using the modified wastegate model, presented in (3.42), is presented together with measured temperatures in Figure 6.5.

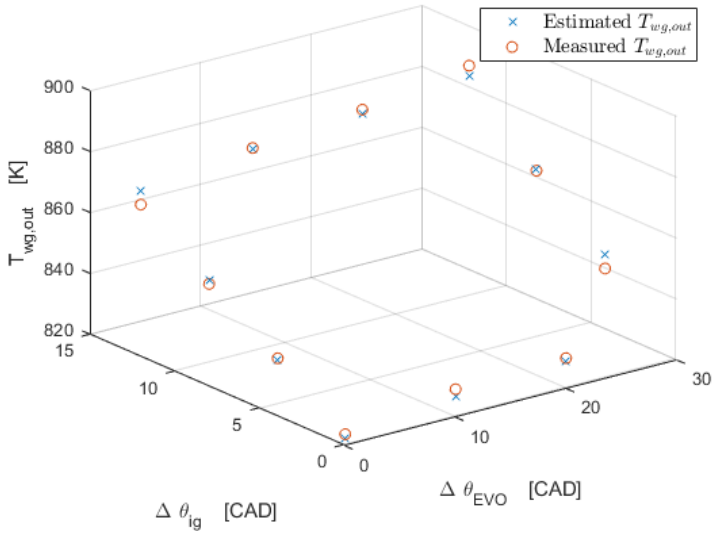

(a) A 3D visualisation of the estimated and measured $T_{wg,out}$ at stationary conditions using the modified model.

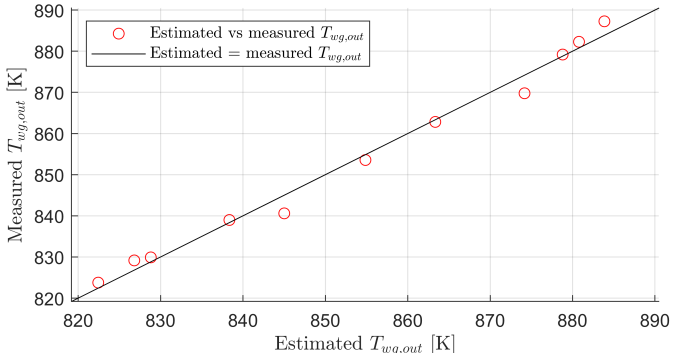

(b) The measured $T_{wg,out}$ plotted against the estimated values at stationary conditions using the modified model.

Figure 6.5: *Visual comparisons between the measured and estimated wastegate out temperatures using the modified model.*

Using the modified wastegate model from (3.42) the MAE is decreased to 1.94 K, or 0.23 %. The improved fit to measurement data motivates the use of the modified model rather than the initial one for the optimal control analysis.

6.5 Pipe temperature loss model

In Figure 6.6 the estimated and measured catalytic converter inlet temperatures are presented for the initial pipe temperature model in (3.45).

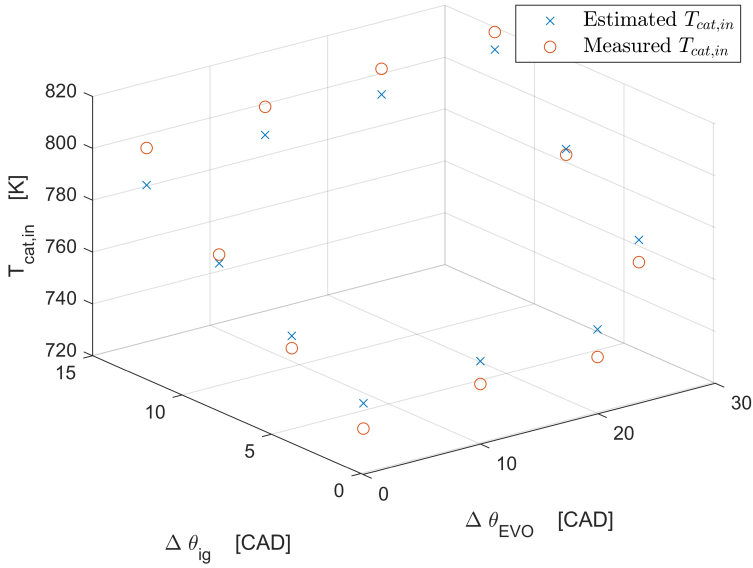

(a) *A 3D visualisation of the estimated and measured catalytic converter inlet temperature at stationary conditions using the initial model.*

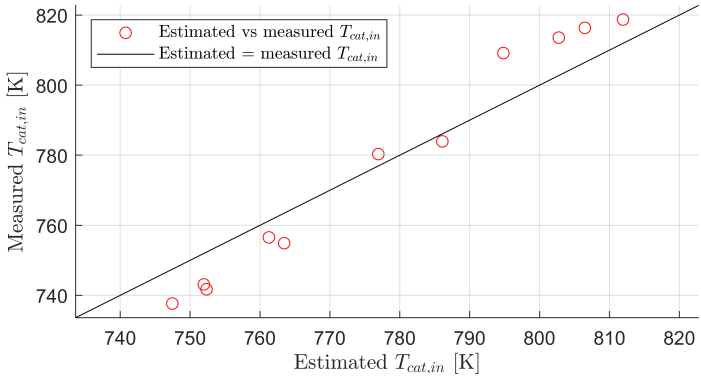

(b) *The measure catalytic converter inlet temperature plotted against the estimated values at stationary conditions using the initial model.*

Figure 6.6: *Visual comparisons between the measured and estimated catalytic converter inlet temperatures using the initial model.*

The MAE for the catalytic converter inlet temperature model is 8.18 K, or 1.05%. The temperatures estimated using the modified pipe temperature model in (3.46) are presented in Figure 6.7 together with measured temperatures.

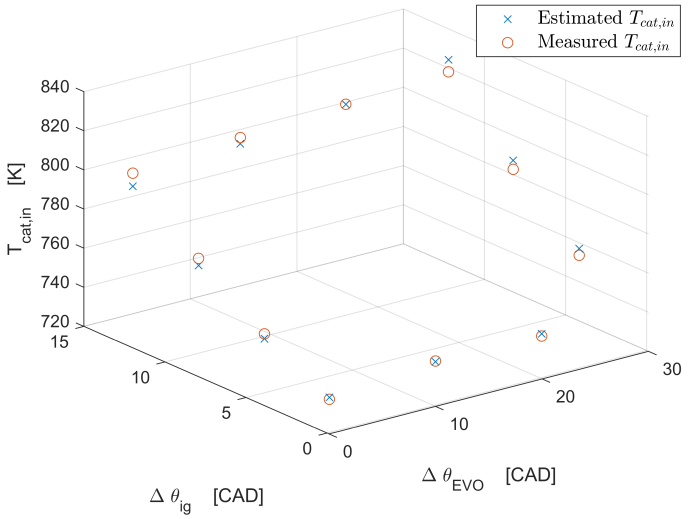

(a) *A 3D visualisation of the estimated and measured catalytic converter inlet temperature at stationary conditions using the modified model.*

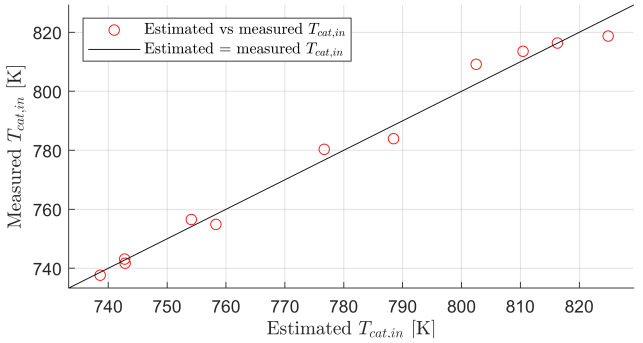

(b) *The measure catalytic converter inlet temperature plotted against the estimated values at stationary conditions using the modified model.*

Figure 6.7: *Visual comparisons between the measured and estimated catalytic converter inlet temperatures using the modified model.*

Using the modified pipe temperature model, the MAE is reduced to 2.95 K, or 0.37%, which motivates using this model over the initial one for the optimal control analysis.

6.6 Catalytic converter temperature model

In Figure 6.8 the measured catalytic converter inlet and outlet temperatures are presented together with the estimated catalytic converter outlet temperature. The model is considered to fit very well to the measured data.

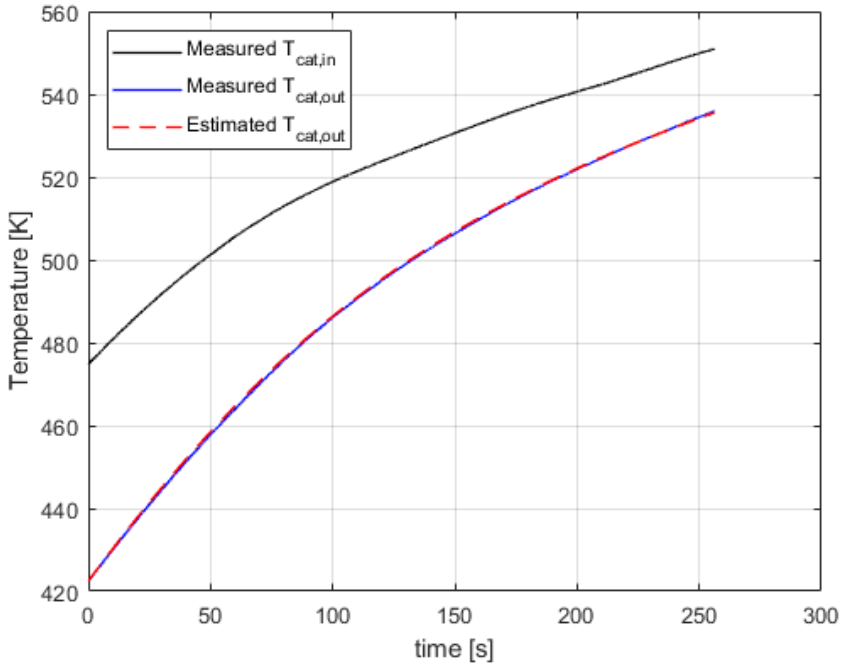

Figure 6.8: *A comparison between estimated and measured values for* $T_{cat,out}$ *during cold start conditions.*

6.7 Exhaust manifold temperature dynamics

In Figure 6.9 the measured and estimated temperatures in the exhaust manifold are presented for a step in ignition angle with fully open wastegate. In the figure the estimated temperature is presented both with no temperature dynamic, and with a time constant of $\tau_{em} = 23$ s.

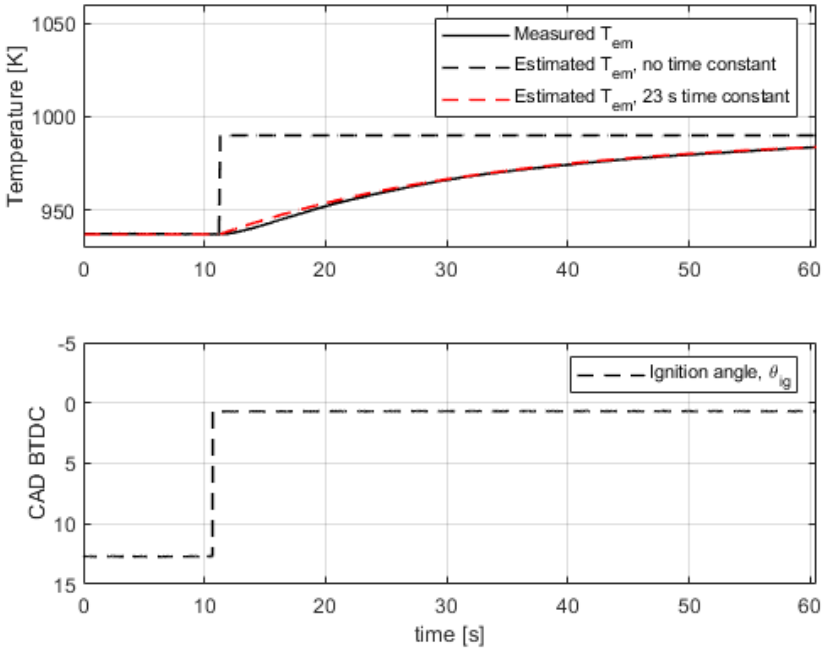

Figure 6.9: *In the top plot measured and estimated exhaust manifold temperatures are presented, and in the bottom plot the corresponding step in ignition angle with fully open wastegate.*

In Figure 6.10 the measured and estimated temperatures in the exhaust manifold is presented for a step in ignition angle with fully closed wastegate. In the figure the estimated temperature is presented both with no temperature dynamic, and with a time constant of $\tau_{em} = 27$ s.

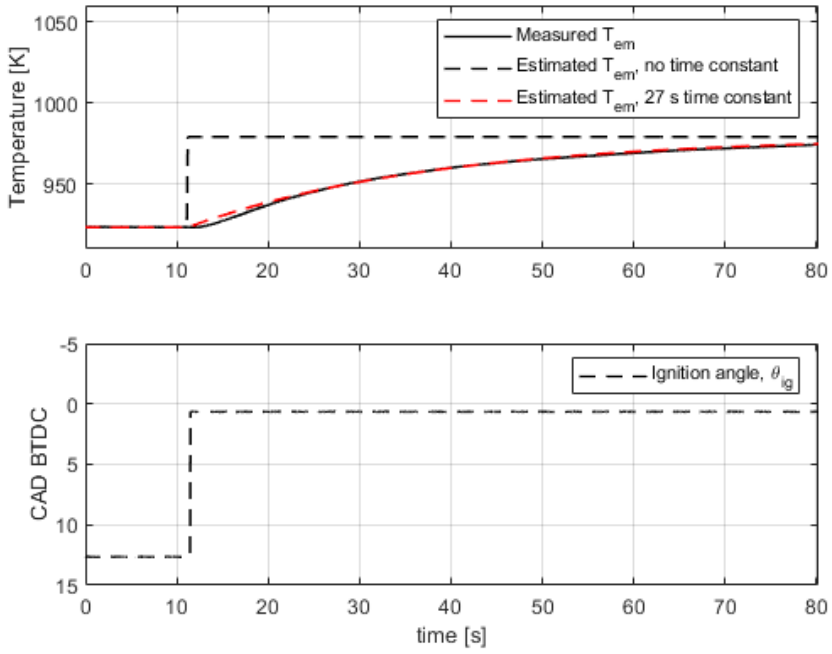

Figure 6.10: *In the top plot measured and estimated exhaust manifold temperatures are presented, and in the bottom plot the corresponding step in ignition angle with fully closed wastegate.*

6.8 Pipe temperature dynamics

The measured and estimated temperatures at the catalytic converter inlet are presented in Figure 6.11 for the step response with closed wastegate. A time constant of $\tau_{pipe} = 8$ seconds is considered giving good fit to measurement data.

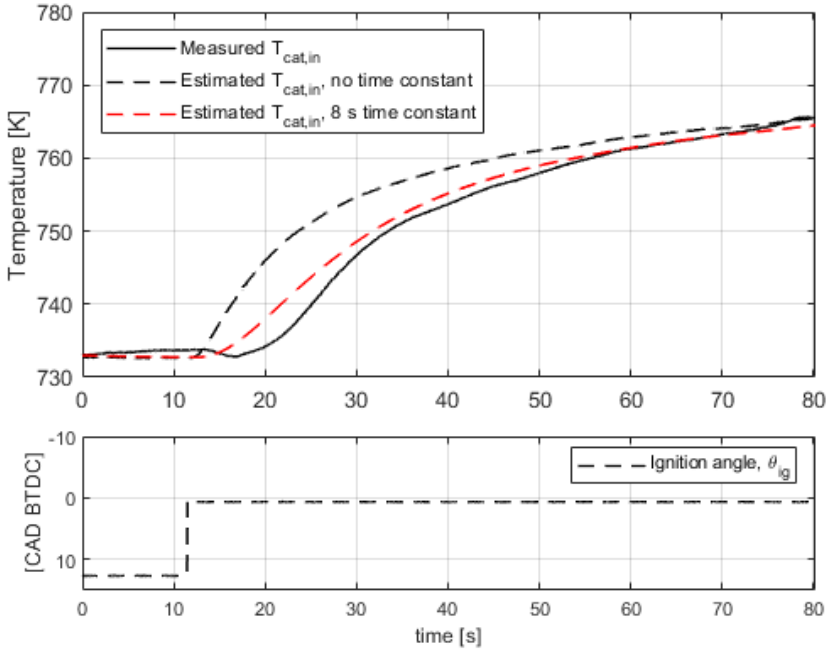

Figure 6.11: *In the top plot measured and estimated catalyst inlet temperatures are presented, and in the bottom plot the corresponding step in ignition angle with fully closed wastegate.*

An attempt was made to also use data from the step response measurement with fully open wastegate to estimate the pipe time constant, but no reasonable result was obtained. It is believed that the reason for this is that the temperature sensor at the turbine outlet on the test engine used for the data collection is positioned in the mass flow in such a way that data obtained during dynamic measurements are possibly unreliable, as reasoned in Section 5.4.

7

Results

This chapter covers the optimal control strategies obtained using the proposed models.

7.1 Fully open wastegate

7.1.1 Variations in θ_{ig} and θ_{evo}

As described in Chapter 4 the system was first simulated with $\Delta\theta_{ig} = \Delta\theta_{evo} = 0$ to obtain reference values for catalytic converter heating time and fuel consumption. The obtained reference heating time is denoted t_{ref} and the reference fuel consumption $m_{f,ref}$. As presented in Chapter 4, optimizations were performed to obtain time and fuel optimal solutions. In addition to these, optimizations were also performed with fixed end times of $t_{final} = 0.85 \cdot t_{ref}$, $t_{final} = 0.90 \cdot t_{ref}$ and $t_{final} = 0.95 \cdot t_{ref}$. The obtained catalytic converter heating times, accumulated fuel consumptions and fuel mass flows are presented in Table 7.1.

Table 7.1: *The obtained catalyst heating times and fuel consumptions for the model with fully open wastegate using control signals $\Delta\theta_{ig}$ and $\Delta\theta_{evo}$.*

t_{final} [s]	m_f [g]	$\dot{m}_f$ [g/s]	t/t_{ref}	$m_f/m_{f,ref}$	$\dot{m}_f/\dot{m}_{f,ref}$	**Comment**
40.77	46.50	1.14	100.0 %	100.0 %	100.0 %	Reference values
38.73	45.53	1.18	95.0 %	97.9 %	103.0 %	Fixed time of 95 % of t_{ref}
36.69	44.79	1.22	90.0 %	96.3 %	107.0 %	Fixed time of 90 % of t_{ref}
34.65	44.38	1.28	85.0 %	95.4 %	112.3 %	Fixed time of 85 % of t_{ref}
34.21	44.36	1.30	83.9 %	95.4 %	113.7 %	Minimized accumulated fuel
34.09	44.36	1.30	83.6 %	95.4 %	114.1 %	Time optimal solution

The data presented in Table 7.1 is also presented graphically in Figure 7.1.

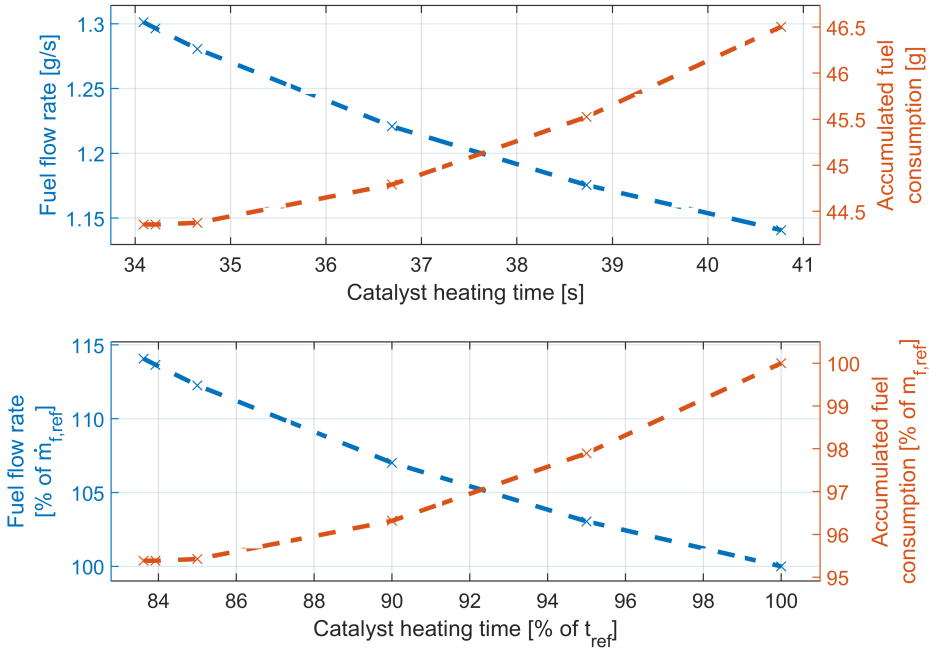

Figure 7.1: *Accumulated fuel consumption and fuel flow rate for fuel optimal solutions for different catalytic converter heating times using control signals $\Delta\theta_{ig}$ and $\Delta\theta_{evo}$.*

The optimal control strategies for the optimization solutions presented in Table 7.1 and Figure 7.1 are presented separately in Figures 7.2 - 7.6. In the figures, temperatures T_{eo}, T_{em}, $T_{cat,in}$ and $T_{cat,out}$ are presented together with exhaust mass flow $\dot{m}_{exh}$ and the control signals θ_{ig} and θ_{evo}. In the figures a distinct phase behaviour can be observed in exhaust mass flow. A high mass flow phase is present which, as the total heating time of the catalytic converter is shortened, is extended over a longer and longer time period.

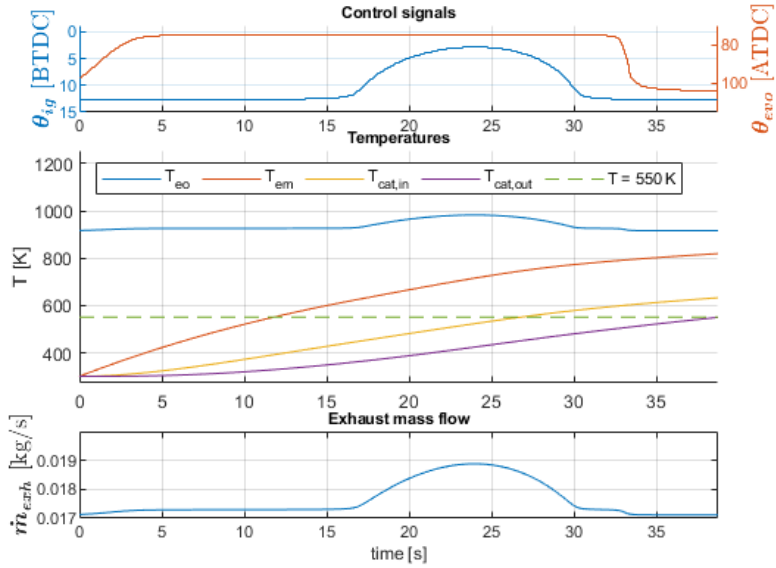

Figure 7.2: *The fuel optimal solution for fixed end time* $t_{final} = 0.95 \cdot t_{ref}$ *and fully open wastegate.*

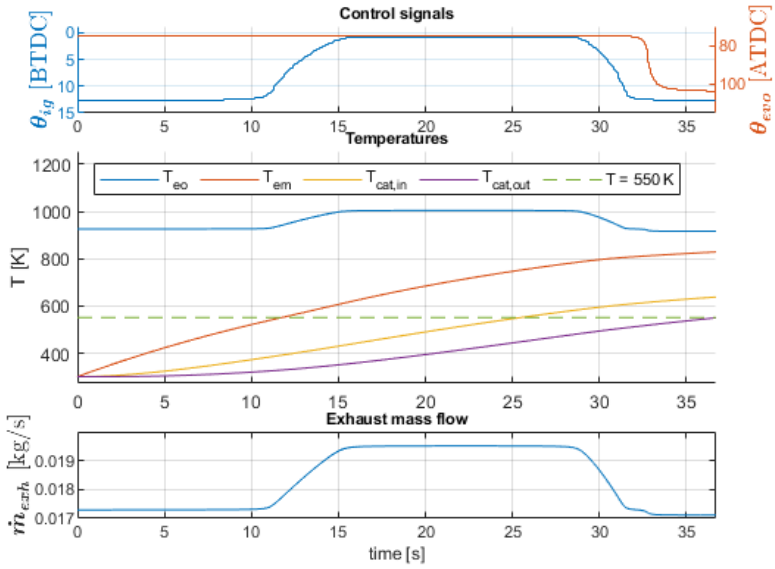

Figure 7.3: *The fuel optimal solution for fixed end time* $t_{final} = 0.90 \cdot t_{ref}$ *with open wastegate.*

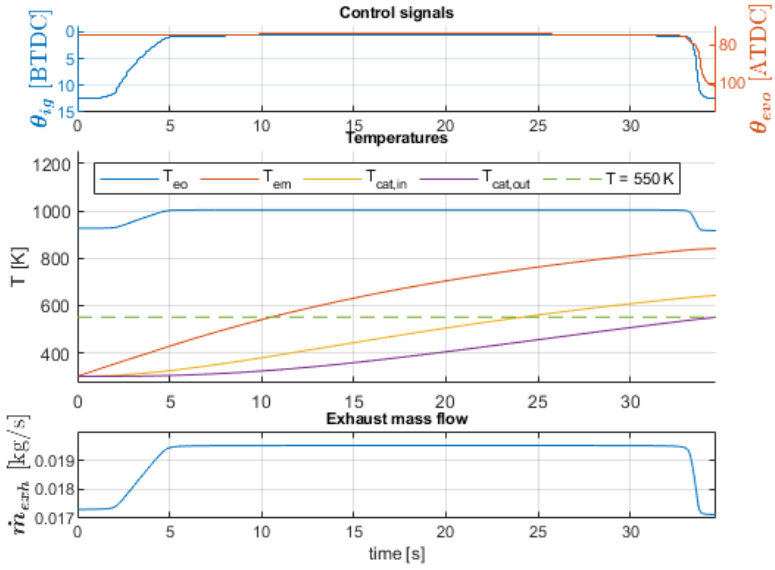

Figure 7.4: *The fuel optimal solution for fixed end time* $t_{final} = 0.85 \cdot t_{ref}$ *with open wastegate.*

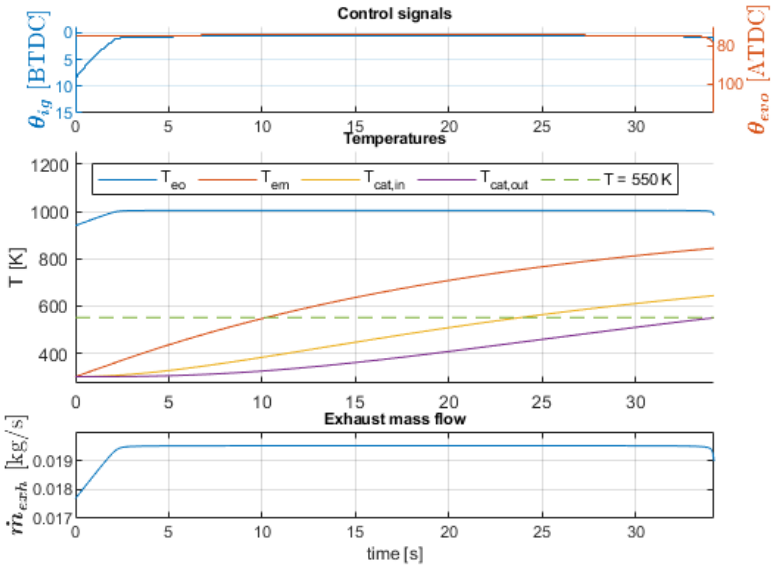

Figure 7.5: *The fuel optimal solution for free end time with open wastegate.*

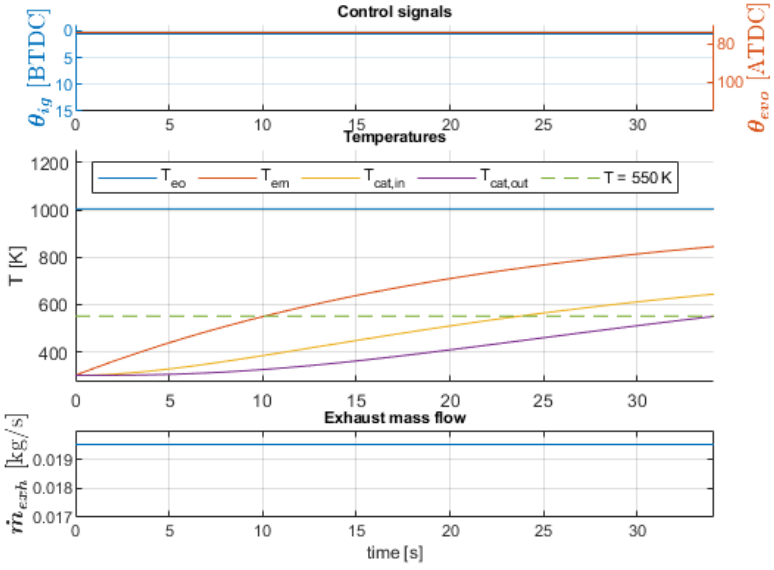

Figure 7.6: *The time optimal solution for model with open wastegate.*

7.1.2 Variations in θ_{ig}, θ_{evo} and λ

The corresponding optimizations as in previous section were performed with λ as an additional control signal. The results from these optimizations are presented in Table 7.2.

Table 7.2: *The obtained catalytic converter heating times and fuel consumptions for the model with fully open wastegate using control signals $\Delta\theta_{ig}$, $\Delta\theta_{evo}$ and λ.*

t_{final} [s]	m_f [g]	$\dot{m}_f$ [g/s]	t/t_{ref}	$m_f/m_{f,ref}$	$\dot{m}_f/\dot{m}_{f,ref}$	**Comment**
40.77	46.50	1.14	100.0 %	100.0 %	100.0 %	Reference values
38.73	43.77	1.13	95.0 %	94.1 %	99.1 %	Fixed time of 95 % of t_{ref}
36.69	42.92	1.17	90.0 %	92.3 %	102.5 %	Fixed time of 90 % of t_{ref}
34.65	42.30	1.22	85.0 %	91.0 %	107.0 %	Fixed time of 85 % of t_{ref}
32.84	42.07	1.28	80.5 %	90.5 %	112.3 %	Minimized accumulated fuel
32.68	42.10	1.29	80.2 %	90.5 %	112.9 %	Time optimal solution

The data presented in Table 7.2 is graphically presented in Figure 7.7.

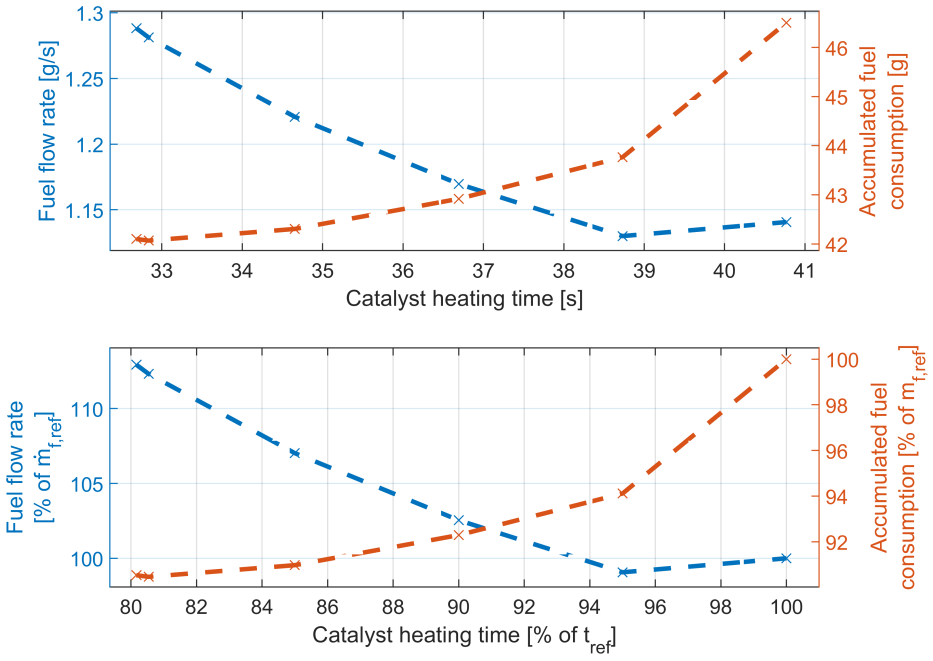

Figure 7.7: *Accumulated fuel consumption and fuel flow rate for fuel optimal solutions for different catalytic converter heating times using control signals $\Delta\theta_{ig}$, $\Delta\theta_{evo}$ and λ.*

The fuel optimal control strategies for the optimization solutions presented in Table 7.2 and Figure 7.7 are presented separately in Figures 7.8 - 7.12. In the figures, temperatures T_{eo}, T_{em}, $T_{cat,in}$ and $T_{cat,out}$ are presented together with exhaust mass flow $\dot{m}_{exh}$ and the control signals θ_{ig}, θ_{evo} and λ. One again a distinct phase behaviour can be observed in exhaust mass flow, whose appearance is evolving as the heating time of the catalytic converter is shortened.

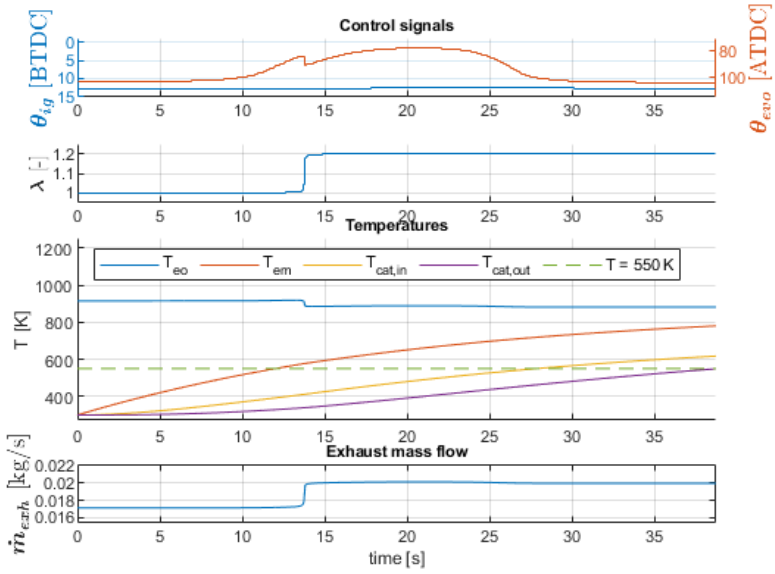

Figure 7.8: *The fuel optimal solution for fixed end time* $t_{final} = 0.95 \cdot t_{ref}$ *and fully open wastegate with variable* λ*.*

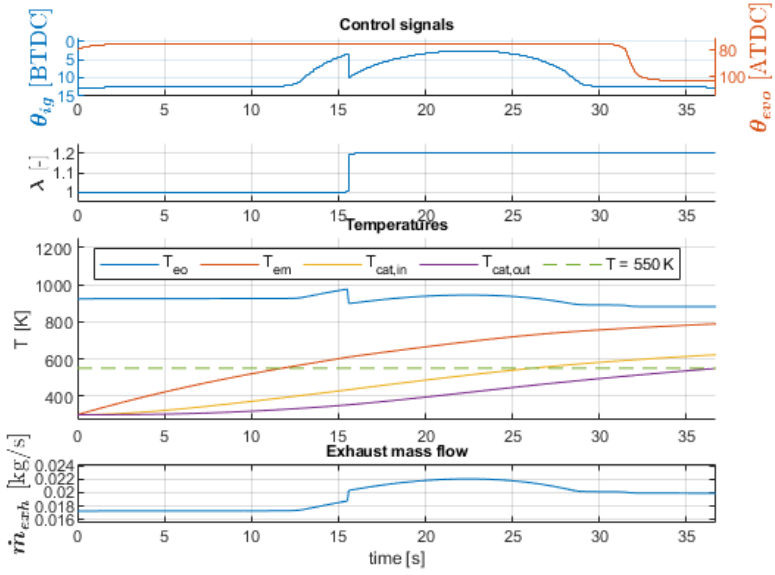

Figure 7.9: *The fuel optimal solution for fixed end time* $t_{final} = 0.90 \cdot t_{ref}$ *and fully open wastegate with variable* λ*.*

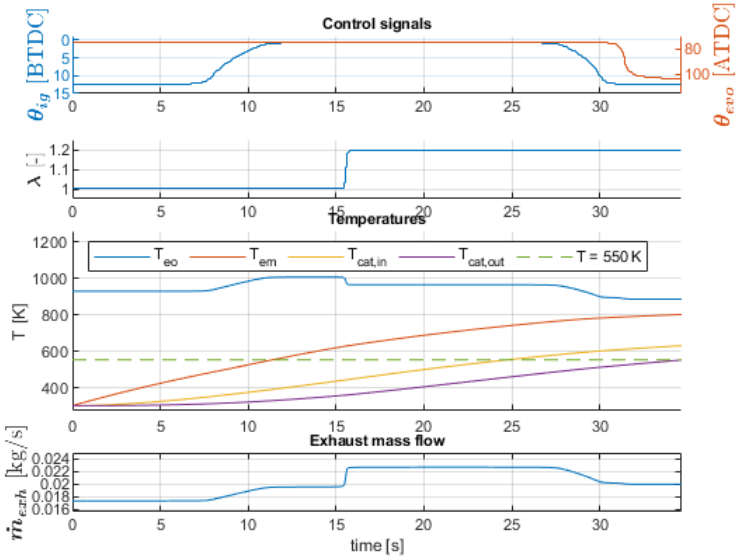

Figure 7.10: *The fuel optimal solution for fixed end time* $t_{final} = 0.85 \cdot t_{ref}$ *and fully open wastegate with variable* λ.

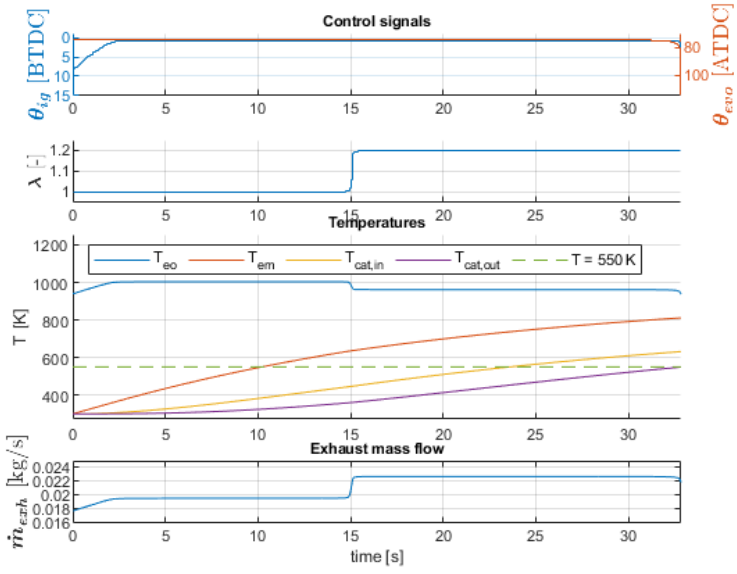

Figure 7.11: *The fuel optimal solution for free end time and fully open wastegate with variable* λ.

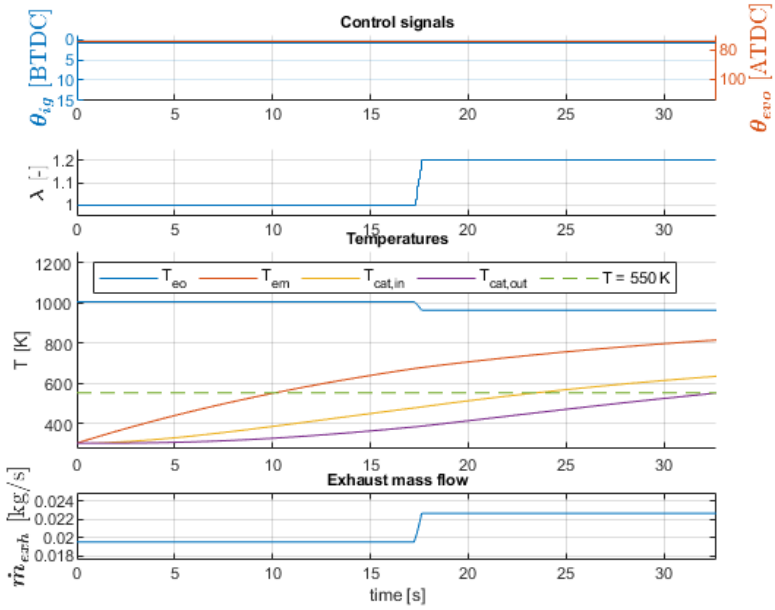

Figure 7.12: *The time optimal solution for model with fully open wastegate with variable λ.*

7.2 Fully closed wastegate

For the model with fully closed wastegate the corresponding optimizations were performed as for the model with fully open wastegate in Section 7.1.

7.2.1 Variations in θ_{ig} and θ_{evo}

Table 7.3: *The obtained catalytic converter heating times and fuel consumptions for the model with fully open wastegate using control signals $\Delta\theta_{ig}$ and $\Delta\theta_{evo}$.*

t_{final} [s]	m_f [g]	$\dot{m}_f$ [g/s]	t/t_{ref}	$m_f/m_{f,ref}$	$\dot{m}_f/\dot{m}_{f,ref}$	**Comment**
40.44	46.13	1.14	100.0 %	100.0 %	100.0 %	Reference values
38.42	45.15	1.18	95.0 %	97.9 %	103.0 %	Fixed time of 95 % of t_{ref}
36.40	44.39	1.22	90.0 %	96.2 %	106.9 %	Fixed time of 90 % of t_{ref}
34.37	43.98	1.28	85.0 %	95.3 %	112.2 %	Fixed time of 85 % of t_{ref}
34.05	43.97	1.29	84.2 %	95.3 %	113.2 %	Minimized accumulated fuel
33.79	43.97	1.30	83.6 %	95.3 %	114.1 %	Time optimal solution

The data presented in Table 7.3 is also presented graphically in Figure 7.13.

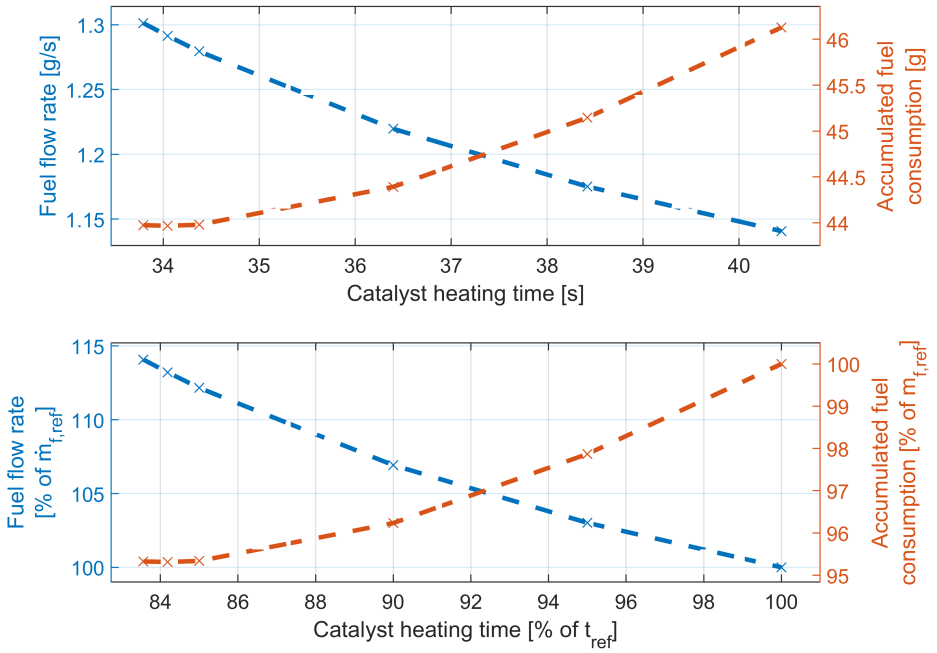

Figure 7.13: *Accumulated fuel consumption and fuel flow rate for fuel optimal solutions for different catalytic converter heating times with closed wastegate using control signals $\Delta\theta_{evo}$ and $\Delta\theta_{ig}$.*

The fuel optimal control strategies for the optimization solutions presented in Table 7.3 and Figure 7.13 are presented separately in Figures 7.14 - 7.18. In the figures, temperatures T_{eo}, T_{em}, $T_{cat,in}$ and $T_{cat,out}$ are presented together with exhaust mass flow $\dot{m}_{exh}$ and the control signals θ_{ig} and θ_{evo}. As for the case with open wastegate, a distinct phase behaviour can be observed in exhaust mass flow, which is affected by the heating time of the catalytic converter.

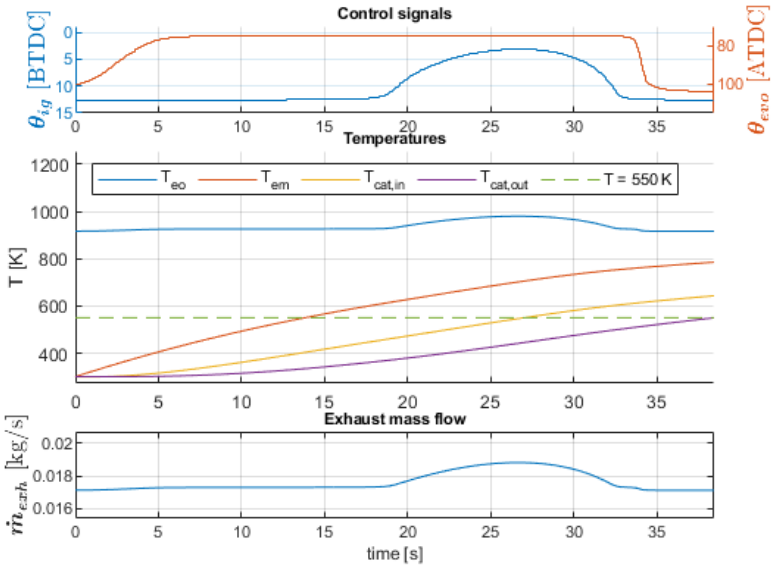

Figure 7.14: *The fuel optimal solution for fixed end time* $t_{final} = 0.95 \cdot t_{ref}$ *and fully closed wastegate.*

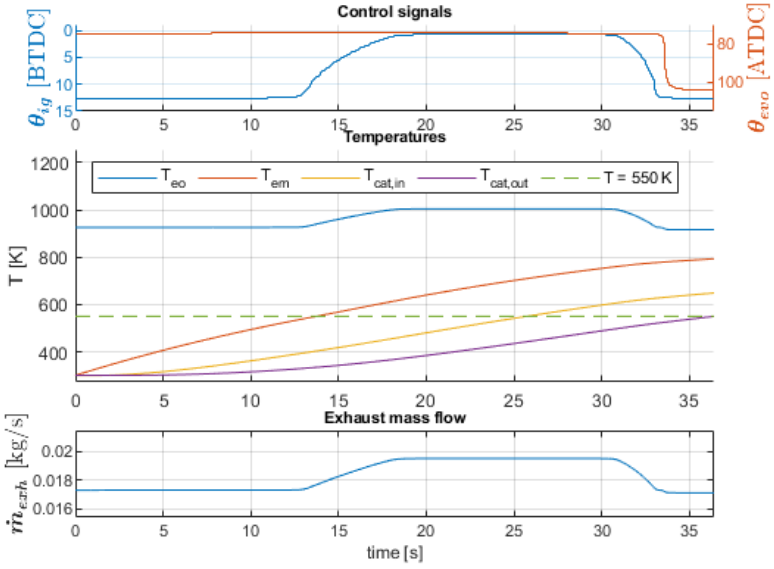

Figure 7.15: *The fuel optimal solution for fixed end time* $t_{final} = 0.90 \cdot t_{ref}$ *and fully closed wastegate.*

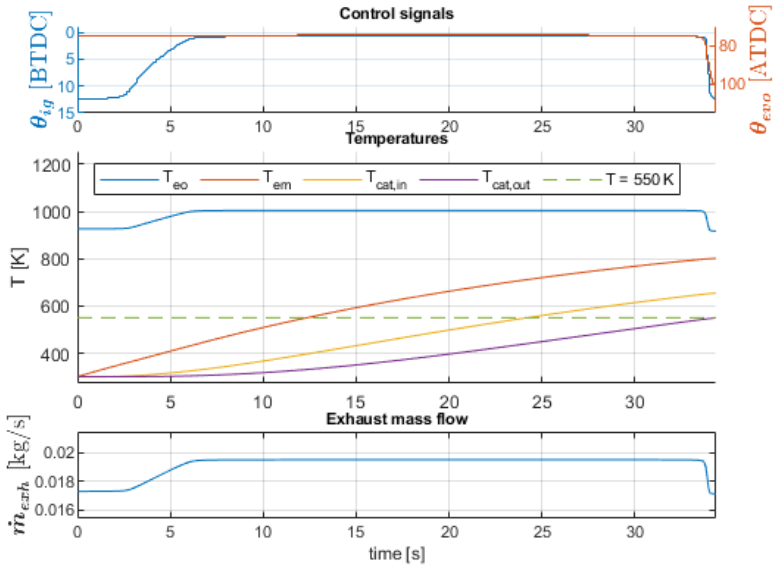

Figure 7.16: *The fuel optimal solution for fixed end time* $t_{final} = 0.85 \cdot t_{ref}$ *and fully closed wastegate.*

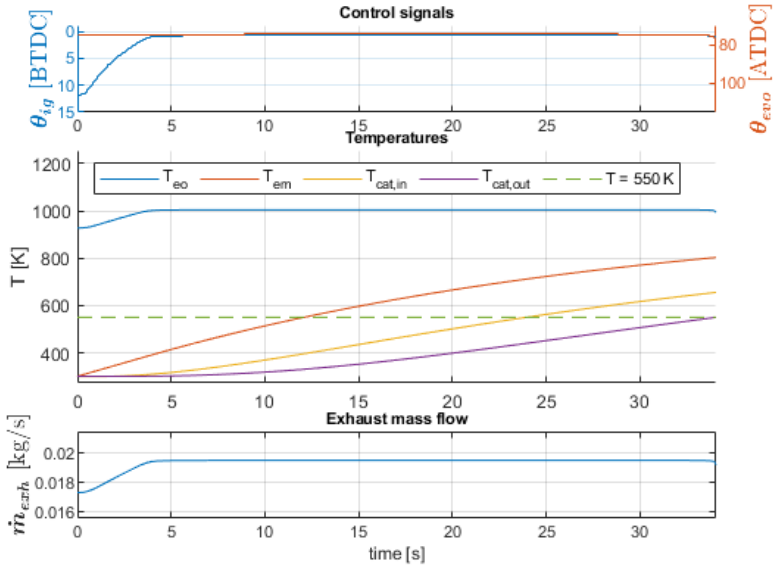

Figure 7.17: *The fuel optimal solution for free end time and fully closed wastegate.*

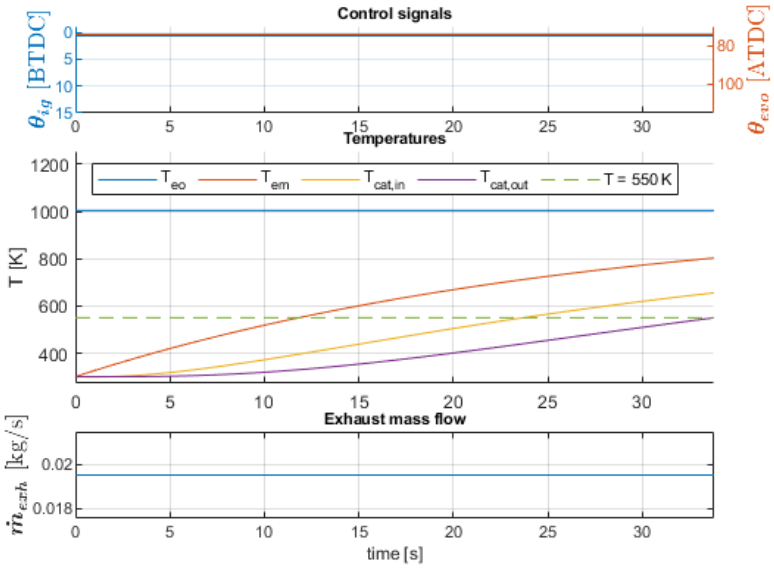

Figure 7.18: *The time optimal solution for model with fully closed wastegate.*

7.2.2 Variations in θ_{ig}, θ_{evo} and λ

The corresponding optimizations as in previous section were performed with λ as an additional control signal. The results from these optimizations are presented in Table 7.4.

Table 7.4: *The obtained catalytic converter heating times and fuel consumptions for the model with closed wastegate using control signals $\Delta\theta_{ig}$, $\Delta\theta_{evo}$ and λ.*

t_{final} [s]	m_f [g]	$\dot{m}_f$ [g/s]	t/t_{ref}	$m_f/m_{f,ref}$	$\dot{m}_f/\dot{m}_{f,ref}$	**Comment**
40.44	46.13	1.14	100.0 %	100.0 %	100.0 %	Reference values
38.42	43.28	1.13	95.0 %	93.8 %	98.8 %	Fixed time of 95 % of t_{ref}
36.40	42.42	1.17	90.0 %	92.0 %	102.2 %	Fixed time of 90 % of t_{ref}
34.37	41.85	1.22	85.0 %	90.7 %	106.7 %	Fixed time of 85 % of t_{ref}
32.59	41.61	1.28	80.6 %	90.2 %	111.9 %	Minimized accumulated fuel
32.33	41.65	1.29	79.9 %	90.3 %	113.0 %	Time optimal solution

The data presented in Table 7.4 is graphically presented in Figure 7.19.

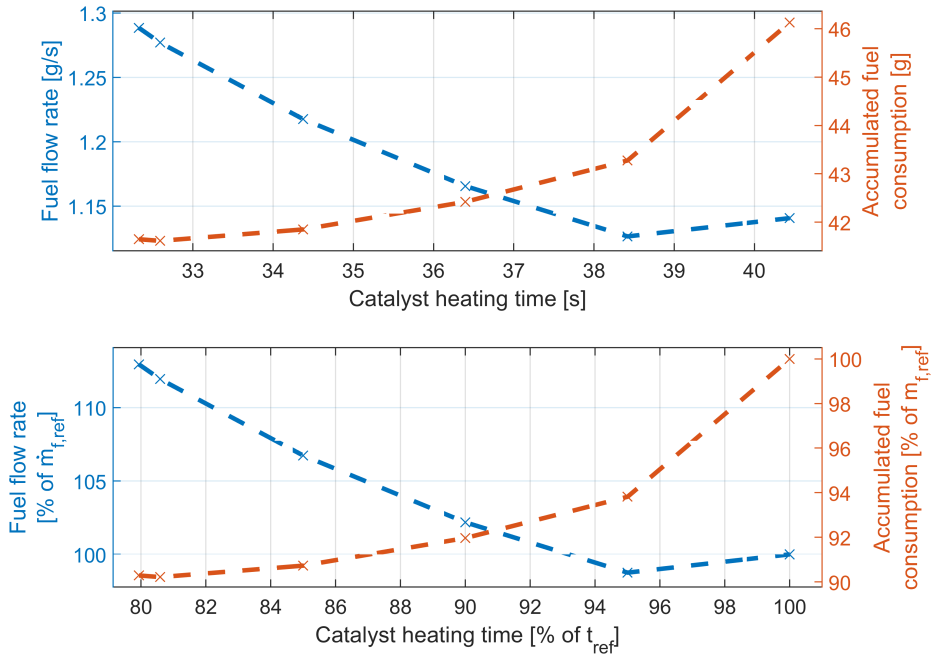

Figure 7.19: *Accumulated fuel consumption and fuel flow rate for fuel optimal solutions for different catalytic converter heating times with variable λ and closed wastegate.*

The fuel optimal control strategies for the optimization solutions presented in Table 7.4 and Figure 7.19 are presented separately in Figures 7.20 - 7.24. In the figures, temperatures T_{eo}, T_{em}, $T_{cat,in}$ and $T_{cat,out}$ are presented together with exhaust mass flow $\dot{m}_{exh}$ and the control signals θ_{ig}, θ_{evo} and λ. One again a distinct phase behaviour can be observed in exhaust mass flow. As the heating of the catalytic converter is shortened, the appearance of the exhaust mass flow phase is evolving similarly to what can be observed for case with open wastegate and variable lambda, section 7.1.2.

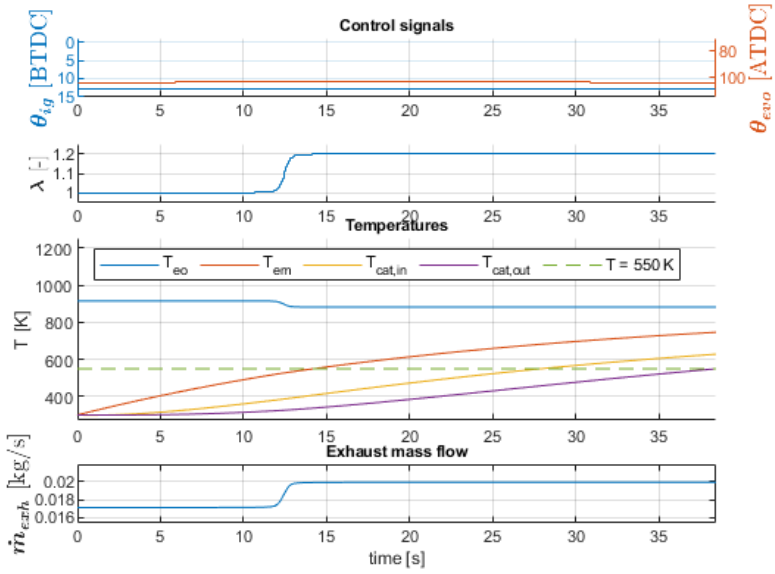

Figure 7.20: *The fuel optimal solution for fixed end time* $t_{final} = 0.95 \cdot t_{ref}$ *and fully closed wastegate with variable* λ.

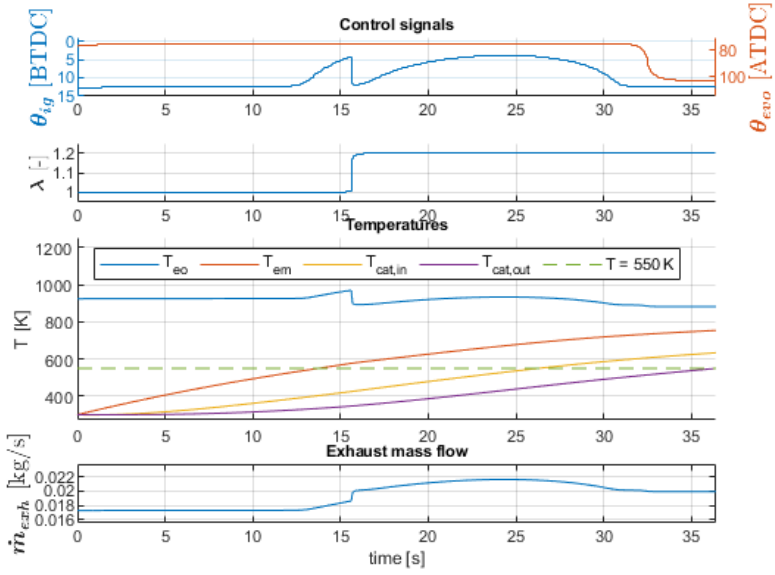

Figure 7.21: *The fuel optimal solution for fixed end time* $t_{final} = 0.90 \cdot t_{ref}$ *and fully closed wastegate with variable* λ.

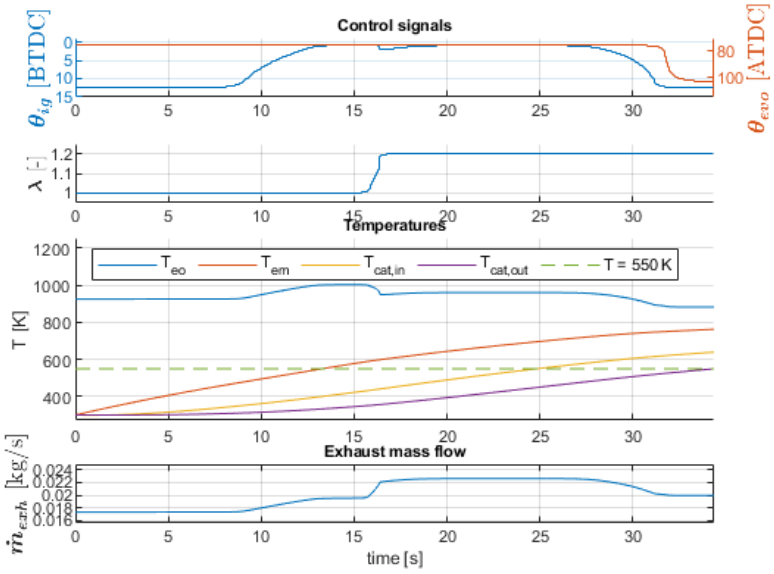

Figure 7.22: *The fuel optimal solution for fixed end time* $t_{final} = 0.85 \cdot t_{ref}$ *and fully closed wastegate with variable* λ*.*

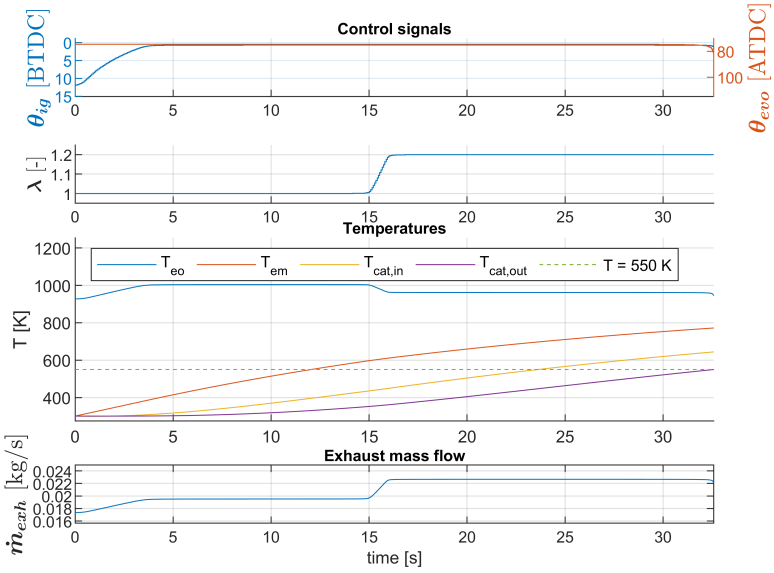

Figure 7.23: *The fuel optimal solution for free end time and fully closed wastegate with variable* λ*.*

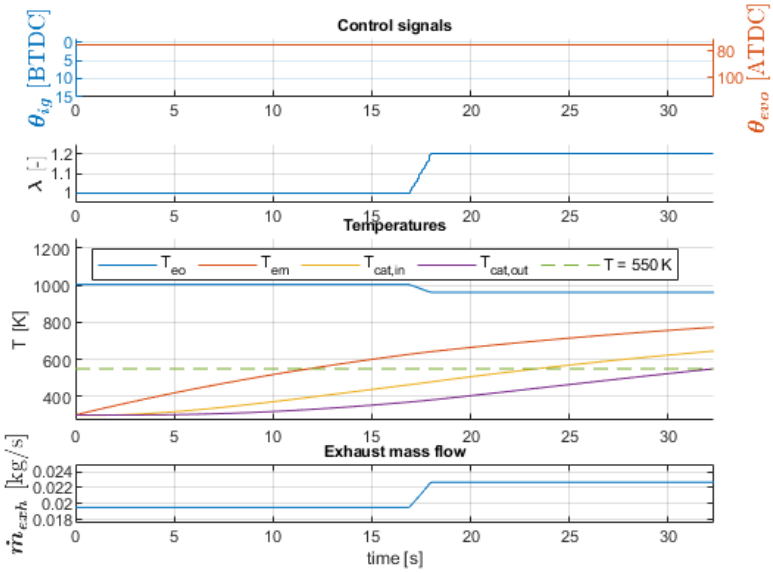

Figure 7.24: *The time optimal solution for model with fully closed wastegate with variable λ.*

8

Discussion, conclusions and future work

8.1 Discussion

In this section the presented work is discussed. The discussion is divided into two sections. In the first section the discussion is focused on the modelling work, including thoughts on the used approach as well as the accuracy of the obtained models. In the second section thoughts on the obtained optimal control strategies are presented.

8.1.1 Modelling

The main objective of the modelling within this project has been to obtain exhaust temperature and mass flow models where ignition and exhaust valve opening angles are included. This has been achieved by using the ideal Otto cycle as the base of the cylinder model, and introduce suitable modifications to include variations in ignition and exhaust valve opening angles. The modifications that lead to the proposed cycle efficiency model in (3.8b) and pump work model in (3.10), in Section 3.2, have not been observed in any of the previous research presented in Chapter 2. The proposed models for cylinder out temperature and exhaust mass flow include the modified cycle, and have proven to give good fit to measurement data in the model validation, Chapter 6.

In the cylinder model the angles θ_{MB50} and θ_{evo} are modelled as first order polynomials of the deviations from nominal values, see (3.4). The variations in cylinder out temperature and mass flow due to variations in ignition and exhaust valve opening angles are well captures by the model, see Figures 6.1 and 6.2 in Chapter 6, indicating that using the first order polynomials as approximations of the angles is a suitable approach to use. Reasonably, even better fit to measurement data should be achieved by increasing the order of the polynomials in (3.4). This,

however, has not been investigated in this project.

In several of the submodels presented in Chapter 3 simple relationships have been assumed. For example, in (3.26) and (3.36) proportionality have been assumed between different temperatures, and in (3.39) a linear relationship is assumed between a temperature and mass flow rate, which is not necessarily physically correct. These assumptions have still been proven to result in models well fitting to measurement data, as shown in Chapter 6, but leaves a lot of room for further model development. In this project the model parameters have only been estimated to fit data for one constant speed-torque operating point. Reasonably, these assumptions might need to be replaced if the models are to be extended to be valid for a wider range of engine speeds and load torques.

The dynamic temperature models have been shown to capture the main dynamic temperature behaviour in both the exhaust manifold and the pipe section between turbine outlet and catalytic converter inlet. When estimating the first order time constants some error is likely introduced since no sensor dynamics have been taken into account. Having an error in the model introduced due to neglecting the sensor is, however, not considered to be a major issue since the primary interest of this project is the optimal control strategy, not modeling the exhaust temperature with the highest possible accuracy.

When including the first order time constants in the models, the main dynamic temperature behaviour is captured, but it is believed that better accuracy can be obtained with further developed models. For example, the temperature dynamics in the pipe section between the turbine and catalytic converter appears to have a time delay in its step response, which is not captured by the proposed dynamic model. However, a further developed dynamic temperature model could possibly capture this phenomenon.

In general, the proposed models in Chapter 3 are considered to give a good fit to measurement data in Chapter 6.

8.1.2 Optimal control strategies

From the results presented in Chapter 7 it is clear that both the heating time of the catalytic converter and the accumulated fuel consumption can be improved both by controlling $\Delta\theta_{ig}$ and $\Delta\theta_{evo}$ alone, and in combination with λ.

Using $\Delta\theta_{ig}$ and $\Delta\theta_{evo}$ alone a distinct behaviour can be seen in exhaust mass flow for both cases with open and closed wastegate. An initial phase with low mass flow is succeeded by a phase with higher mass flow. Observing the control signals it can be seen that the ignition angle has the major influence on the mass flow when λ is fixed, while the exhaust valve opening angle has a minor effect. A clear pattern is that the exhaust valve has a long phase with early opening, while the ignition angle has a similar phase with late ignition but during a shorter time

period.

When λ is included as a control signal along with $\Delta\theta_{ig}$ and $\Delta\theta_{evo}$ a similar phase behaviour can still be observed in exhaust mass flow. An interesting observation is that λ also exhibits a distinct two phase behaviour for both time and fuel optimal solutions. In the initial phase λ maintains its lower boundary value, before ramping up to the upper boundary value for the second phase. This behaviour can be observed for all optimization solutions where λ has been utilized as a control signal.

8.2 Conclusions

In this thesis it has been shown that the proposed models for exhaust gas temperatures give good fit to measurement data when parameterized for a constant speed-torque operating point. The approach of originating the cylinder model from the ideal Otto cycle has been proven as feasible. By introducing modifications to the ideal Otto cycle the variations in temperature and exhaust mass flow due to variations in ignition and exhaust valve opening angles have been well captured by the proposed cylinder model.

It has also been shown that utilizing variations in ignition and exhaust valve opening angles can be beneficial with the intention of heating the catalytic converter in the most fuel and time effective ways. According to the optimizations performed in this project, the heating time of the catalytic converter for the open wastegate model can be reduced by 16.4% and the accumulated fuel to reach the desired temperature can be reduced by 5.6% compared to the reference values. For the model with closed wastegate the corresponding figures are 16.5% and 5.7%. By further introducing variations in λ, the heating time can be reduced by 19.8% and the accumulated fuel consumption by 9.5% for the model with open wastegate. For the model with closed wastegate the heating time can be reduced by 20.1% and the accumulated fuel consumption by 9.8% when λ is used as an additional control signal.

In general, the optimal control strategies obtained in this project share some close similarities with the result presented in [13]. Especially, similar phase behaviour can be observed in exhaust mass flow.

8.3 Future work

Several directions can be taken in a future continuation of the work presented in this thesis. Presented in this section are some areas that the author of this thesis believes should be of focus in future work.

- Further development of the models by replacing the simple assumptions,

e.g. temperature proportionalities, with more physically based models. The models can also be improved to model pressure dynamics in, for example, the exhaust manifold. Reasonably, this should make the models more valid for a wider range of engine speeds and load torques.

- The obtained optimal trajectories for $\Delta\theta_{ig}$, $\Delta\theta_{evo}$ and λ can be applied as control signals in an engine test bench. This would allow comparisons between optimization results and real world measurement data regarding fuel consumption and heating time. Such comparisons can further validate the models, as well as indicate whether or not the phase behaviour observed in the optimization solutions yield the expected improvements in a real world exhaust system.

- Another interesting continuation of this thesis would be to complement the catalytic converter model with additional models for the various catalytic reactions in the catalytic converter with respect to temperature. The catalytic converter temperature model used in this project allows the catalytic converter to be divided into segments, and thus the chemical conversions in each of the segments can be modelled. By doing this the objective function in (4.19) could be reformulated to minimize the accumulated emissions rather than fuel consumption. By analyzing the solutions to such optimizations some interesting results can possibly be obtained. For example, it would be of interest to investigate if such optimization solutions would yield the same phase behaviour as observed in this thesis.

- A final suggestion on future work is to combine the proposed models in this thesis with a test drive cycle. Doing this, it would be possible to analyze the optimal heating strategies during variations in engine speed and load torque, and analyze if these variations affect the optimal control strategies for the different control signals.

Appendix

A

Appendix

Derivation of cycle efficiency

The derivation of the cycle efficiency (3.8b) is presented below.

Efficiency is defined as:

$$\eta = \frac{\dot{W}_{out}}{\dot{W}_{in}} = \frac{q_{in} - q_{loss}}{q_{in}} \tag{A.1}$$

With

$$\begin{cases} q_{in} = c_v \cdot (T_3 - T_2) & \text{(A.2a)} \\ q_{loss} = c_v \cdot (T_4 - T_1) & \text{(A.2b)} \end{cases}$$

we obtain:

$$\eta = \frac{c_v \cdot (T_3 - T_2) - c_v \cdot (T_4 - T_1)}{c_v \cdot (T_3 - T_2)} = 1 - \frac{T_4 - T_1}{T_3 - T_2} \tag{A.3}$$

For isentropic compression and expansion the following temperature relationships hold,

$$\begin{cases} T_2 = {r_{comp}}^{\gamma - 1} \cdot T_1 & \text{(A.4a)} \\ T_3 = {r_{exp}}^{\gamma - 1} \cdot T_4 & \text{(A.4b)} \end{cases}$$

where r_{comp} and r_{exp} are defined according to (3.7). (A.5) is obtained by inserting (A.4) into (A.3).

$$\eta = 1 - \frac{T_4 - T_1}{{r_{exp}}^{\gamma-1} \cdot T_4 - {r_{comp}}^{\gamma-1} \cdot T_1} \tag{A.5}$$

Using (A.4a) temperature T_4 can be expressed according to (A.6).

$$T_4 = {r_{exp}}^{1-\gamma} \cdot T_3 \tag{A.6}$$

The temperature T_3 can be expressed as the temperature T_2 with an added term representing the chemical energy released during the isochoric combustion of the fuel, according to (A.7)

$$\begin{aligned} T_3 &= T_2 + \frac{q_{in}}{c_v} = T_2 + \frac{m_f \cdot q_{LHV}}{(m_{air} + m_f) \cdot c_v} \\ &= T_2 + \frac{q_{LHV}}{(1 + (\frac{A}{F})_s \cdot \lambda) \cdot c_v} \end{aligned} \tag{A.7}$$

Inserting (A.4a) into (A.7) and combining with (A.6), the temprerature T_4 can be expressed in terms of T_1 according to (A.8).

$$T_4 = {r_{exp}}^{1-\gamma} \cdot \left(T_1 \cdot {r_{comp}}^{\gamma-1} + \frac{q_{LHV}}{(1 + (\frac{A}{F})_s \cdot \lambda) \cdot c_v} \right) \tag{A.8}$$

By inserting (A.8) into (A.5) the efficiency expression in (A.9) is obtained.

$$\eta = 1 - \frac{{r_{exp}}^{1-\gamma} \cdot \left(T_1 \cdot {r_{comp}}^{\gamma-1} + \frac{q_{LHV}}{(1+(\frac{A}{F})_s \cdot \lambda) \cdot c_v} \right) - T_1}{{r_{exp}}^{\gamma-1} \cdot {r_{exp}}^{1-\gamma} \cdot \left(T_1 \cdot {r_{comp}}^{\gamma-1} + \frac{q_{LHV}}{(1+(\frac{A}{F})_s \cdot \lambda) \cdot c_v} \right) - {r_{comp}}^{\gamma-1} \cdot T_1} =$$

$$= \ldots =$$

$$= 1 - {r_{exp}}^{1-\gamma} - \frac{(1 - \frac{A}{F}_s \cdot \lambda) \cdot c_v}{q_{LHV}} \cdot \left({r_{comp}}^{\gamma-1} - {r_{exp}}^{\gamma-1} \right) \cdot {r_{exp}}^{1-\gamma} \cdot T_1 \tag{A.9}$$

Finally, by using the definitions of r_{comp} and r_{exp} from (3.7),

$$\begin{cases} r_{comp} = \dfrac{V_d + V_c}{V_{MB50}} \\ r_{exp} = \dfrac{V_{evo}}{V_{MB50}} \end{cases}$$

expression (A.10) can be obtained from (A.9),

$$\eta = 1 - \left(\frac{V_{MB50}}{V_{evo}}\right)^{\gamma-1} - \frac{(1-(A/F)_s \cdot \lambda)\cdot c_v}{q_{LHV}} \cdot \left(\left(\frac{V_c + V_d}{V_{evo}}\right)^{\gamma-1} - 1\right) \cdot T_{im} \qquad \text{(A.10)}$$

which is the expresssion presented in (3.8b).

Bibliography

[1] Habib Aghaali and Hans-Erik Angström. Temperature estimation of turbocharger working fluids and walls under different engine loads and heat transfer conditions. *SAE Technical Paper*, (2013-24-0123), 2013.

[2] A.H.Kakaee, M. H. Shojaeefard, and J. Zareei. Sensitivity and effect of ignition timing on the performance of a spark ignition engine: An experimental andmodeling study. *Journal of Combustion*, (doi:10.1155/2011/678719), 2011.

[3] Joel A E Andersson, Joris Gillis, Greg Horn, James B Rawlings, and Moritz Diehl. CasADi – A software framework for nonlinear optimization and optimal control. *Mathematical Programming Computation*, In Press, 2018.

[4] D.I Andrianov, C. Manzie, and M.J Brear. Spark ignition engine control strategies for minimising cold start fuel consumption under cumulative tailpipe emissions constraints. 2013.

[5] Delphine Bresch-Pietri, Thomas Leroy, and Nicolas Petit. Control-oriented time-varying input-delayed temperature model for si engine exhaust catalyst. 2013.

[6] Moritz Diehl. Numerical optimal control. 07 2011.

[7] Lars Eriksson. Mean value models for exhaust system temperatures. *SAE Technical Paper*, (2002-01-0374), 2002.

[8] Lars Eriksson and Ingemar Andersson. An analytic model for cylinder pressure in a four stroke engine. *SAE Technical Paper*, (2002-01-0371), 2002.

[9] Jonathan W. Fox, Wai K. Cheng, and John B. Heywood. A model for predicting residual gas fraction in spark-ignition engines. *SAE Technical Paper*, (931025), 1993.

[10] C. Guardiola, P. Olmeda, B. Pla, and P. Bares. In-cylinder pressure based model for exhaust temperature estimation in internal combustion engines. *Elsevier*, 2016.

[11] Raffael Hedinger, Philipp Elbert, and Christopher Onder. Optimal cold-start control of a gasoline engine. *Energies*, 10(10), 2017.

[12] John B. Heywood. Internal combustion engine fundamentals. *McGraw-Hill series in mechanical engineering*, 1988.

[13] Olov Holmer and Lars Eriksson. Modeling and analytical solutions for optimal heating of aftertreatment systems. 2019.

[14] Lee Kyu Hyun, Shim Chang Yeul, and Kim Wan-Bum. Development of dual wall air gap exhaust system. *SAE Technical Paper*, (2000-01-0205), 2000.

[15] A. H. Kakaeea and J. Zareeib. Influence of varying timing angle on performance of an si engine: An experimental and numerical study. 2013.

[16] M. Kang and T. Shen. Experimental comparisons between lqr and mpc for spark-ignition engine control problem. 2017.

[17] J.T.B.A. Kessels, D.L. Foster, and W.A.J. Bleuanus. Fuel penalty comparison for (electrically) heated catalyst technology. 2010.

[18] F. Keynejad and C. Manzie. Suboptimal cold start strategies for spark ignition engines. *IEEE Transactions on Control Systems Technology*, 2013.

[19] T. Leroy, G. Alix, J. Chauvin, A. Duparchy, and F. Le Berr. Modeling fresh air charge and residual gas fraction on a dual independent variable valve timing si engine. *SAE International*, (2008-01-0983), 2008.

[20] Waibhaw H. Meshram, S.P. Chincholkar, Vikas I. Somankar, and J.G. Suryawanshi. Ignition timing investigation on the performance and emissions of spark ignition engine fuelled with gasoline. (ISSN: 2321-8169), 2017.

[21] Michael Mladek and Christopher H. Onder. A model for the estimation of inducted air mass and the residual gas fraction using cylinder pressure measurements. *SAE Technical Paper Series*, (2000-01-0958), 2000.

[22] Paul Moraal and Ilya Kolmanovsky. Turbocharger modeling for automotive control applications. *SAE Technical Paper*, (1999-01-0908), 1999.

[23] Lars Nielsen and Lars Eriksson. Modeling and control of engines and drivelines. *Wiley, 2014, ISBN: 978-1-118-47999-5*, (2013-24-0123), 2013.

[24] S. Koteswara Rao, Rayees Imam, Karthik Ramanathan, and S. Pushpavanam. Sensitivity analysis and kinetic parameter estimation in a three way catalytic converter. 2009.

[25] Alessandro Romagnoli and Ricardo Martinez-Botas. Heat transfer analysis in a turbocharger turbine: An experimental and computational evaluation. 2012.

[26] Stefano Sabatini, Irfan Kil, Joseph Dekar, Travis Hamilton, Jeff Wuttke, Michael A Smith, Mark A Hoffman, and Simona Onori. A new semi-empirical temperature model for the three way catalytic converter. 2015.

[27] Josefin Storm. Heat transfer modeling for turbocharger control. (LiTH-ISY-EX–17/5098–SE), 2017.

[28] Lukas Tunka and Adam Polcar. Effect of various ignition timings on combustion process and performance of gasoline engine. 2017.

[29] Andreas Wächter and Lorenz T. Biegler. On the implementation of an interior-point filter line-search algorithm for large-scale nonlinear programming. *Mathematical Programming*, 2006. ISSN 1436-4646. doi: 10.1007/s10107-004-0559-y.

[30] Saïd Zidat and Michael Parmentier. Exhaust manifold design to minimize catalyst light-off time. *SAE Technical Paper*, (2000-01-0205), 2000.

[31] Per Öberg and Lars Eriksson. Control oriented modeling of the gas exchange process in variable cam timing engines. *SAE Technical Paper*, (2006-01-0660), 2006.